Article

Current Biology

# Identification of *Chlamydomonas* Central Core Centriolar Proteins Reveals a Role for Human WDR90 in Ciliogenesis

## Highlights

- Mapping of centriolar sub-regions using structured illumination microscopy
- Relative quantitative mass spectrometry reveals novel centriolar components
- Identification of *Chlamydomonas* central core proteins POB15 and POC16
- POC16 and its human homolog WDR90 promote flagella/cilia formation

## Authors

Virginie Hamel, Emmanuelle Steib, Romain Hamelin, ..., Michel O. Steinmetz, Paul Guichard, Pierre Gönczy

## Correspondence

paul.guichard@unige.ch (P. Guichard), pierre.gonczy@epfl.ch (P. Gönczy)

## In Brief

The composition and function of the central core region of centrioles is ill defined. Using mass spectrometry and super-resolution microscopy, Hamel et al. discover POB15 and POC16 as two *Chlamydomonas* central core components. They further establish that POC16 and its human homolog WDR90 are required for efficient flagella/cilia formation.

Hamel et al., 2017, Current Biology *27*, 2486–2498
August 21, 2017 
http://dx.doi.org/10.1016/j.cub.2017.07.011

CellPress

CellPress

Current Biology
Article

# Identification of *Chlamydomonas* Central Core Centriolar Proteins Reveals a Role for Human WDR90 in Ciliogenesis

Virginie Hamel,[1,6] Emmanuelle Steib,[2] Romain Hamelin,[3] Florence Armand,[3] Susanne Borgers,[2] Isabelle Flückiger,[1] Coralie Busso,[1] Natacha Olieric,[4] Carlos Oscar S. Sorzano,[5] Michel O. Steinmetz,[4] Paul Guichard,[1,6,*] and Pierre Gönczy[1,7,*]

[1]Swiss Institute for Experimental Cancer Research (ISREC), School of Life Sciences, Swiss Federal Institute of Technology (EPFL), Lausanne 1015, Switzerland
[2]Department of Cell Biology, Sciences III, University of Geneva, Geneva 1211, Switzerland
[3]Proteomic Core Facility and Technology Platform, Swiss Federal Institute of Technology (EPFL), Lausanne 1015, Switzerland
[4]Laboratory of Biomolecular Research, Division of Biology and Chemistry, Paul Scherrer Institut, Villigen 5232, Switzerland
[5]Biocomputing Unit, Centro Nacional de Biotecnologia, CSIC, Campus de Cantoblanco, Darwin 3, 28049 Madrid, Spain
[6]Present address: Department of Cell Biology, Sciences III, University of Geneva, Geneva 1211, Switzerland
[7]Lead Contact
*Correspondence: paul.guichard@unige.ch (P. Guichard), pierre.gonczy@epfl.ch (P. Gönczy)
http://dx.doi.org/10.1016/j.cub.2017.07.011

## SUMMARY

Centrioles are evolutionarily conserved macromolecular structures that are fundamental to form cilia, flagella, and centrosomes. Centrioles are 9-fold symmetrical microtubule-based cylindrical barrels comprising three regions that can be clearly distinguished in the *Chlamydomonas reinhardtii* organelle: an ~100-nm-long proximal region harboring a cartwheel; an ~250-nm-long central core region containing a Y-shaped linker; and an ~150-nm-long distal region ending at the transitional plate. Despite the discovery of many centriolar components, no protein has been localized specifically to the central core region in *Chlamydomonas* thus far. Here, combining relative quantitative mass spectrometry and super-resolution microscopy on purified *Chlamydomonas* centrioles, we identified POB15 and POC16 as two proteins of the central core region, the distribution of which correlates with that of tubulin glutamylation. We demonstrated that POB15 is an inner barrel protein within this region. Moreover, we developed an assay to uncover temporal relationships between centriolar proteins during organelle assembly and thus established that POB15 is recruited after the cartwheel protein CrSAS-6 and before tubulin glutamylation takes place. Furthermore, we discovered that two *poc16* mutants exhibit flagellar defects, indicating that POC16 is important for flagellum biogenesis. In addition, we discovered that WDR90, the human homolog of POC16, localizes to a region of human centrioles that we propose is analogous to the central core of *Chlamydomonas* centrioles. Moreover, we demonstrate that WDR90 is required for ciliogenesis, echoing the findings in *Chlamydomonas*. Overall, our work provides novel insights into the identity and function of centriolar central core components.

## INTRODUCTION

Centrioles and the related basal bodies are crucial for the proper execution of fundamental processes, such as cell signaling and motility, as well as cell polarity and spindle assembly [1, 2]. Centrioles are barrel-shaped structures ~500 nm long and ~250 nm in diameter characterized by a 9-fold radial arrangement of microtubules [3, 4]. Cryo-tomography of *Chlamydomonas* basal bodies (hereafter referred to as centrioles for simplicity) revealed three regions that each display specific ultrastructural features [5]: first, a proximal region containing a cartwheel important for organelle assembly; second, a region termed the central core; and third, a more distal region that connects the organelle to the transition zone. Of particular importance to this work, the central core region harbors the so-called Y-shaped linker, an inner barrel-like structure located adjacent to the inside face of centriolar microtubules, which has been hypothesized to act as a scaffold stabilizing the centriole wall [5]. An analogous structure has been observed in purified human centrioles but, in this case, in a more distal region of the organelle [6, 7]. Whereas the identity of several proteins residing in the cartwheel-bearing region and in the distal-most region of centrioles is known, this is not the case for the central core region of *Chlamydomonas* centrioles.

Over the last 15 years, an increasing number of centriolar proteins have been identified, including through mass spectrometry studies, and several of them have been localized within the centriole, notably in the cartwheel-bearing region, the microtubule wall, and the centriolar lumen [8–14]. *Chlamydomonas* has been particularly instrumental for discovering centriolar proteins because, in contrast to most other systems, centrioles in this species are essentially devoid of pericentriolar material (PCM) [15], thus constituting an optimal sample for proteomic identification of centriolar components.

 

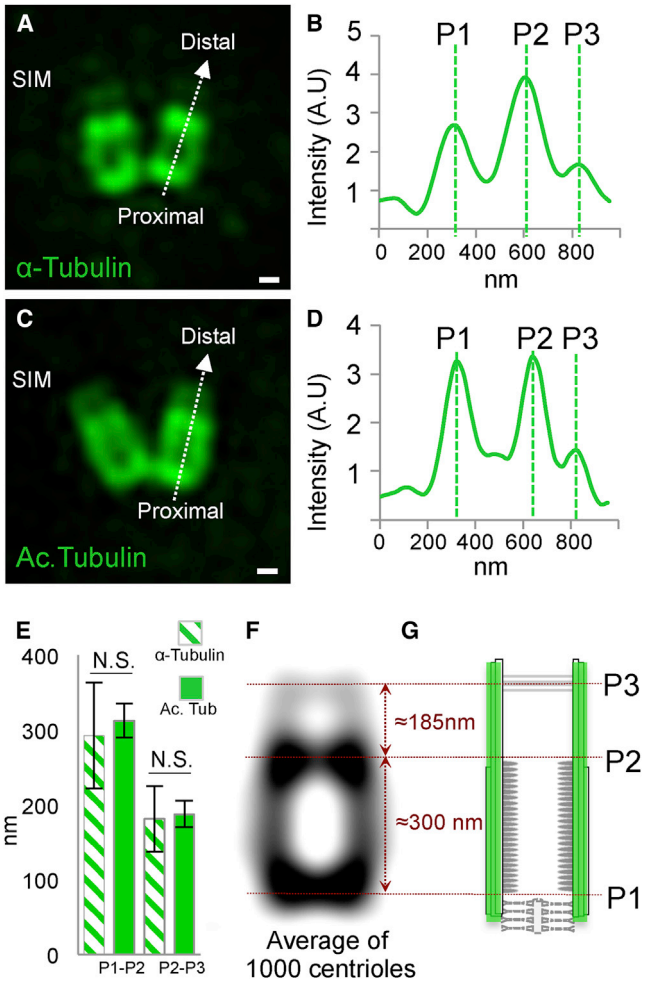


**Figure 1. Mapping of Centriolar Regions Using Super-Resolution Microscopy**

(A and C) Structured illumination microscopy (SIM) images of isolated *Chlamydomonas* centrioles stained with α-tubulin (A) or acetylated tubulin (C). Arrows in this and other figures indicate the axis along which the plot profiles (shown in B and D in this case) were generated. The scale bars represent 100 nm.

(B and D) Plot profiles of α-tubulin (B) and acetylated tubulin (D), highlighting peaks of fluorescence intensity (P1, P2, and P3).

(E) Distances from P1 to P2 and from P2 to P3 for tubulin and acetylated tubulin. P1 to P2: 292 ± 71 nm for α-tubulin and 313 ± 22 nm for acetylated tubulin; P2 to P3: 181 ± 44 nm for α-tubulin and 188 ± 17 nm for acetylated tubulin. Error bars represent the SD.

(F and G) 3D reconstruction of *Chlamydomonas* centrioles obtained by averaging ~1,000 centrioles stained with acetylated tubulin and imaged using SIM (F), with corresponding schematic representation (G).

See also Figure S1.

A previous proteomic analysis of isolated *Chlamydomonas* centrioles revealed a number of POC (proteome of centriole) proteins [8]. Despite the advances brought by that work, the centriolar protein Bld12p/CrSAS-6 (hereafter referred to as CrSAS-6), a key component of the cartwheel [16], was not detected in that study because the entire cartwheel structure had been lost during sample preparation [5, 15]. This raises the possibility that other important centriolar components could have been missed in that initial study. Moreover, novel proteomic methods are available and a new assembly of the *Chlamydomonas* genome has been released [17]. Importantly, in addition, the exact distribution of most proteins identified previously by proteomic analysis of *Chlamydomonas* centrioles is not known.

In this study, using relative quantitative mass spectrometry for protein discovery and super-resolution microscopy for precise localization, we report the identification of two components of the central core region of *Chlamydomonas* centrioles, POB15 (proteome of basal body) and POC16. Moreover, we uncover that POC16 is important for flagellum assembly as two *poc16* mutants display shorter flagella and cannot swim. Moreover, we find that the human ortholog of POC16, WDR90, is required for efficient primary cilium formation.

## RESULTS

### Visualization of *Chlamydomonas* Centriolar Regions

We set out to develop a method based on immunofluorescence to delineate regional boundaries within *Chlamydomonas* centrioles. To this end, we used structured illumination microscopy (SIM), which affords a lateral resolution of ~120 nm [18], and analyzed isolated centrioles concentrated on coverslips to improve imaging quality [19].

Because centrioles are microtubule-based organelles in which tubulin is heavily acetylated [20], we stained isolated centrioles with antibodies against α-tubulin or acetylated tubulin to mark the centriole microtubule wall. SIM imaging revealed the characteristic V-shaped organization of pairs of mature centrioles in *Chlamydomonas* (Figures 1A, 1C, S1A, and S1B). By comparing such SIM images with cryo-microscopy analysis, we could unambiguously identify the proximal region of the two mature centrioles, which are closer to one another than their distal ends (Figures S1C and S1D). SIM imaging uncovered that centrioles were labeled with both antibodies in a non-uniform manner along their proximal-distal axis, with two major fluorescence peaks (P1 and P2) and a more minor one (P3) toward the distal end (Figures 1A–1E and S1A–S1D), suggesting that microtubules in mature centrioles are fully acetylated. A similar pattern was observed when centrioles stained with antibodies against acetylated tubulin were imaged using stimulated emission depletion (STED) microscopy (Figure S1E), indicating that this distribution is not an artifact due to SIM reconstruction. Likewise, SIM imaging of centrioles stained with antibodies directed against another epitope of α-tubulin and coupled to Alexa Fluor 647 yielded an analogous distribution (Figure S1G). Therefore, we speculate that the weaker signal observed between peaks P1 and P2 might reflect decreased accessibility to tubulin in centriolar microtubules, perhaps owing to post-translational modifications of tubulin in that region, whereas the weaker labeling toward the distal end might reflect the transition from microtubule triplets to microtubule doublets [4].

Plot profile analysis along the SIM-imaged centrioles uncovered two major parts: first, an ~300-nm-long part between P1 and P2, comprising the proximal and central core regions, and second, an ~185-nm-long part between P2 and P3, comprising the more distal region and extending into the transition zone

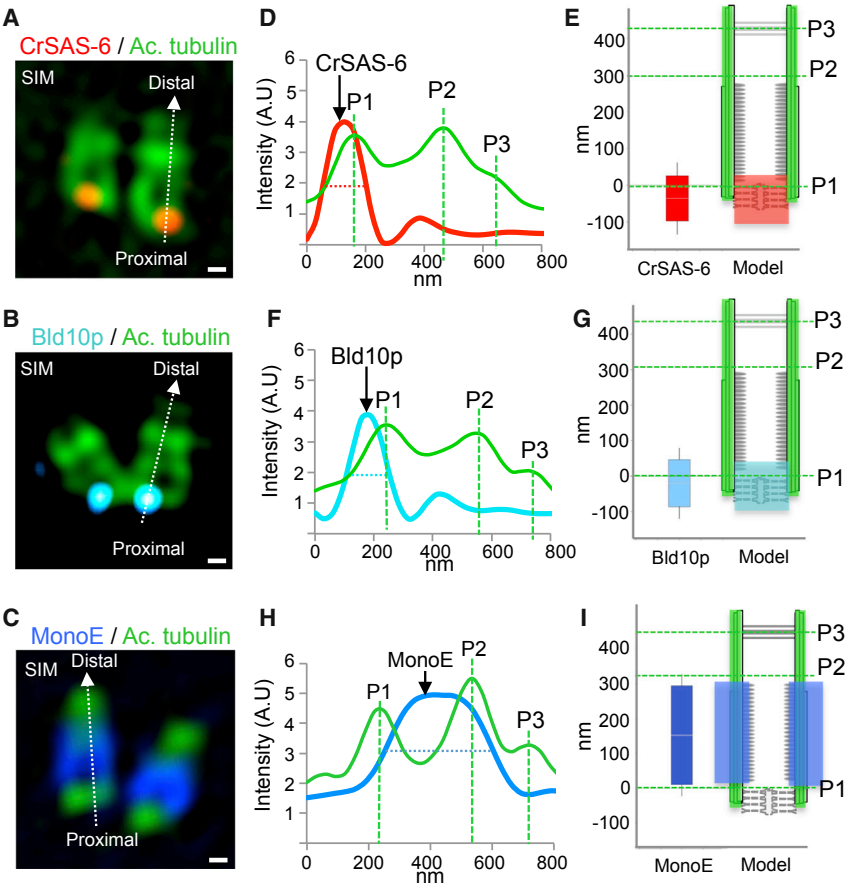


**Figure 2. Localization of Select Centriolar Components**

(A–C) SIM images of purified *Chlamydomonas* centrioles stained with acetylated tubulin (green, all panels), highlighting the proximal localization of the cartwheel components CrSAS-6 (A, red), Bld10p (B, blue), and the central core localization of monoglutamylated tubulin (MonoE; C, dark blue). The scale bars represent 100 nm.

(D, F, and H) Superimposed plot profiles of acetylated tubulin (green) with CrSAS-6 (red) (D), Bld10p (blue) (F), or monoglutamylated tubulin (dark blue) (MonoE) (H).

(E, G, and I) Distribution of CrSAS-6 (E), Bld10p (G), and MonoE (I) as compared to that of acetylated tubulin (left), together with corresponding schematic representations of centriole (right). Heights were as follows: CrSAS-6: 123 ± 20 nm; Bld10p: 133 ± 33 nm; MonoE: 286 ± 33 nm. Error bars represent SD.

See also Figure S1.

(Figures 1B, 1D, and 1E). Single particle analysis of ~1,000 centrioles imaged by SIM allowed the generation of an averaged map of acetylated tubulin staining of *Chlamydomonas* centrioles (Figures 1F and 1G). This provides a reference with precise boundaries for the further mapping of centriolar protein distributions.

We next determined the precise localization of known centriolar components on this reference map, with position "0" being defined as the proximal-most acetylated tubulin signal. We first determined the localizations of CrSAS-6 and Bld10p, two cartwheel components known to be present at the base of the proximal region (Figures 2A and 2B) [16, 21]. Plot profiles relative to the acetylated tubulin reference pattern established that CrSAS-6 and Bld10p signals are each ~120 nm long (Figures 2D–2G). This dimension is in line with the height of the cartwheel observed in mature centrioles by electron microscopy (EM) [3, 4], although we cannot exclude that the actual size may be smaller but appear to be only ~120 nm long, owing to the resolution limit of SIM [18]. Interestingly, in addition, we noted that both CrSAS-6 and Bld10p signals are present ~60 nm below the proximal-most acetylated tubulin signal, raising the possibility that a portion of the cartwheel is not surrounded by microtubules. Such a proximal extension of the cartwheel below microtubules has been observed by cryo-EM in the *Chlamydomonas* procentriole [22], suggesting that it may indeed reflect the native situation.

We searched for components that could mark specifically the central core region. In doing so, we found that monoglutamylated tubulin (MonoE), a post-translational modification of tubulin enriched at centrioles [20], localizes to a region ~280 nm in length and ~200 nm in diameter, constituting a belt in the central core region, between P1 and P2 (Figures 2C, 2H, 2I, S1I, and S1J). A likewise restricted staining was observed for polyglutamylated tubulin (Figures S1I and S1J). We conclude that tubulin modifications are distributed unevenly along the proximal-distal axis of *Chlamydomonas* centrioles.

## Proteomic Analysis of Isolated *Chlamydomonas* Centrioles

We set out to undertake a new proteomic analysis of *Chlamydomonas* centrioles using a milder isolation protocol than previously utilized, thus allowing preservation of the procentriole and of the cartwheel [23] (STAR Methods). In addition, we used dimethyl labeling, which allows one to conduct relative quantitative analysis of protein mixtures present in two samples [24], with the aim of subtracting potential contaminants and identifying bona fide centriolar proteins.

We purified centrioles from *Chlamydomonas* through velocity sedimentation in a sucrose gradient (Figure 3A), ensuring by EM that the procentriole and the cartwheel were present in the material thus isolated (Figure S2A). We determined which gradient fractions were enriched in centrioles using immunofluorescence with antibodies against acetylated tubulin and CrSAS-6 (Figures S2B and S2C). Two independent isolations were performed; fractions enriched in centrioles were mixed into a pool 1 and an equivalent number of fractions devoid of centrioles into a pool 2 (Figures 3A, S2B, S2D, and S2E). Pool 1 and pool 2 samples were then enzymatically digested and the resulting peptides subjected to medium (pool 1) or heavy (pool 2) dimethyl labeling prior to sample mixing and detection of peptides

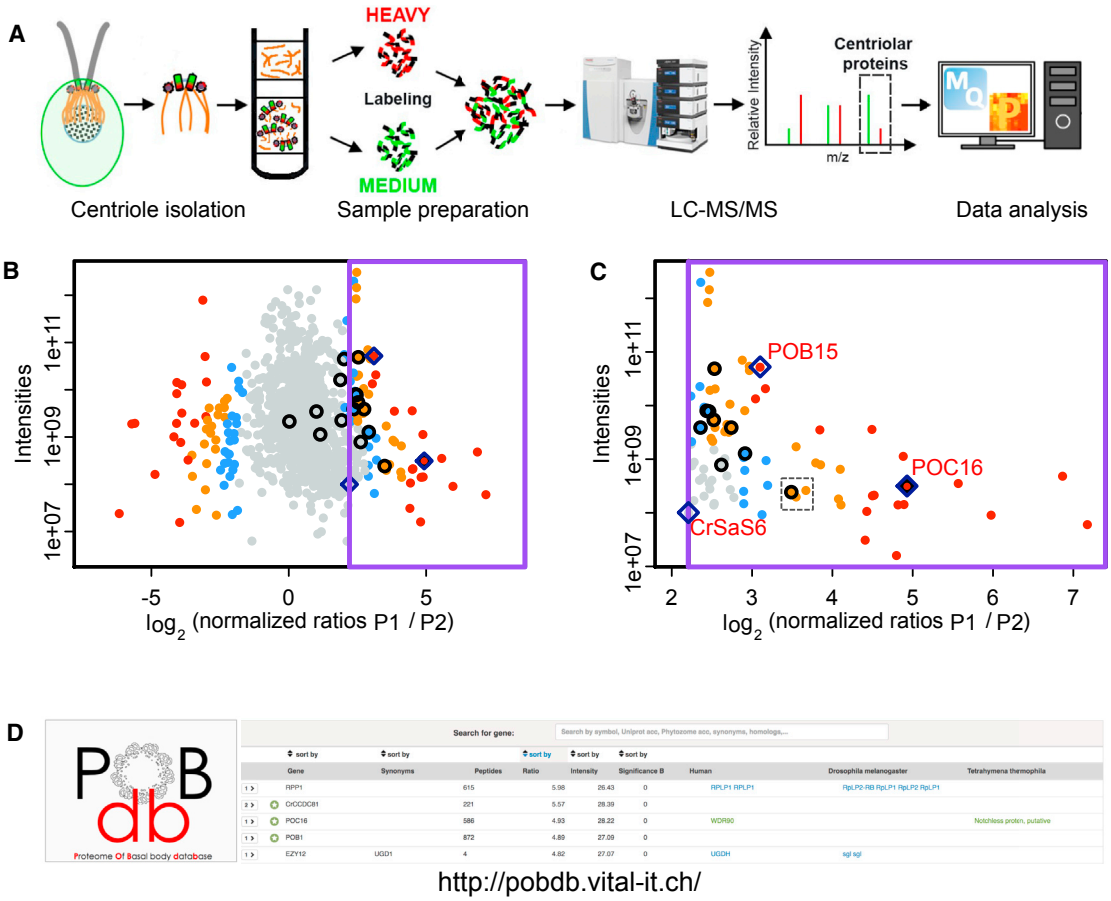


**Figure 3. Proteomic Analysis of Isolated *Chlamydomonas* Centrioles**

(A) Flow chart of mass spectrometry of isolated *Chlamydomonas* centrioles.

(B and C) Semiquantitative mass spectrometry of isolated *Chlamydomonas* centrioles using dimethyl labeling. Black circles (16 in total, some of which are difficult to make out as they are on top of one another), previously identified POC proteins; blue lozenges, CrSAS-6, POB15, and POC16. The purple line designates the cutoff (defined by the position of CrSAS-6), with candidate proteins situated to the right of that (B; magnified in C). The different colors of the discs (gray, orange, and red) correspond to the value of significance B of the mass spectrometry data [25]. Blue, SignB < 0.05; gray, SignB > 0.05; orange, SignB < 0.01; red, SignB < 0.001. Briefly, the red dots in the right part (positive ratios) represent the proteins that are found more in the centriolar fraction than in the contaminant fraction. Note that POB15 and POC16 are among these.

(D) Appearance of the data page of the online POBdb database (http://pobdb.vital-it.ch).

See also Figure S2 and Tables S1 and S2.

by mass spectrometry (Figure 3A; STAR Methods). Figure 3B reports the proteins identified from both samples, with centriole-enriched proteins present toward the right. To evaluate the quality of this centriole protein discovery pipeline, we addressed whether the previously identified POCs were retrieved here. Importantly, we found that this was the case for ~76% of them (i.e., 16/21; Figure 3B, black circles; Table S1). By extension, candidates newly identified here most likely correspond in their majority to proteins enriched at centrioles.

Candidates were ranked according to the $\log_2$ (normalized ratios P1/P2) and the significance B criterion [26] (Table S2). We found that 85 proteins had a $\log_2$ value larger than that of CrSAS-6 and were thus retained for further analysis (Figures 3B and 3C, to the right of the purple line). Among these, 20 proteins with the GO terms metabolism or RNA processing were excluded, as they are less likely to be bona fide resident centriolar components, leaving 65 centriolar protein candidates. We found that 36 of them are predicted to contain a coiled-coil, which is a hallmark of centrosomal proteins [27] (Table S2). Besides POCs, the known centriolar proteins DIP13 [28], BUG23 [8], SF-assemblin [29], Bld10p [30], Tektin [31], and OFD1 [32] were also present, further validating the approach. Note that α- and β-tubulin were also detected but were not particularly enriched in the centriolar fraction ($\log_2$ratioP1/P2 = 1.95 and 1.7; significance B > 0.05), as expected given that microtubule-based ciliary contaminants are present in pool 2. Moreover, among the 65 selected candidates, we found that 27 have clear human homologs (Table S2). Of these, 19 were previously identified in a centrosome mass spectrometry analysis [33]. Unless they had a previous designation, we termed the new candidates on this list POBs, for proteome of basal body, thus distinguishing them from the previously identified POCs [8].

In order to render this mass spectrometry analysis most useful for the scientific community, we developed a dynamic online

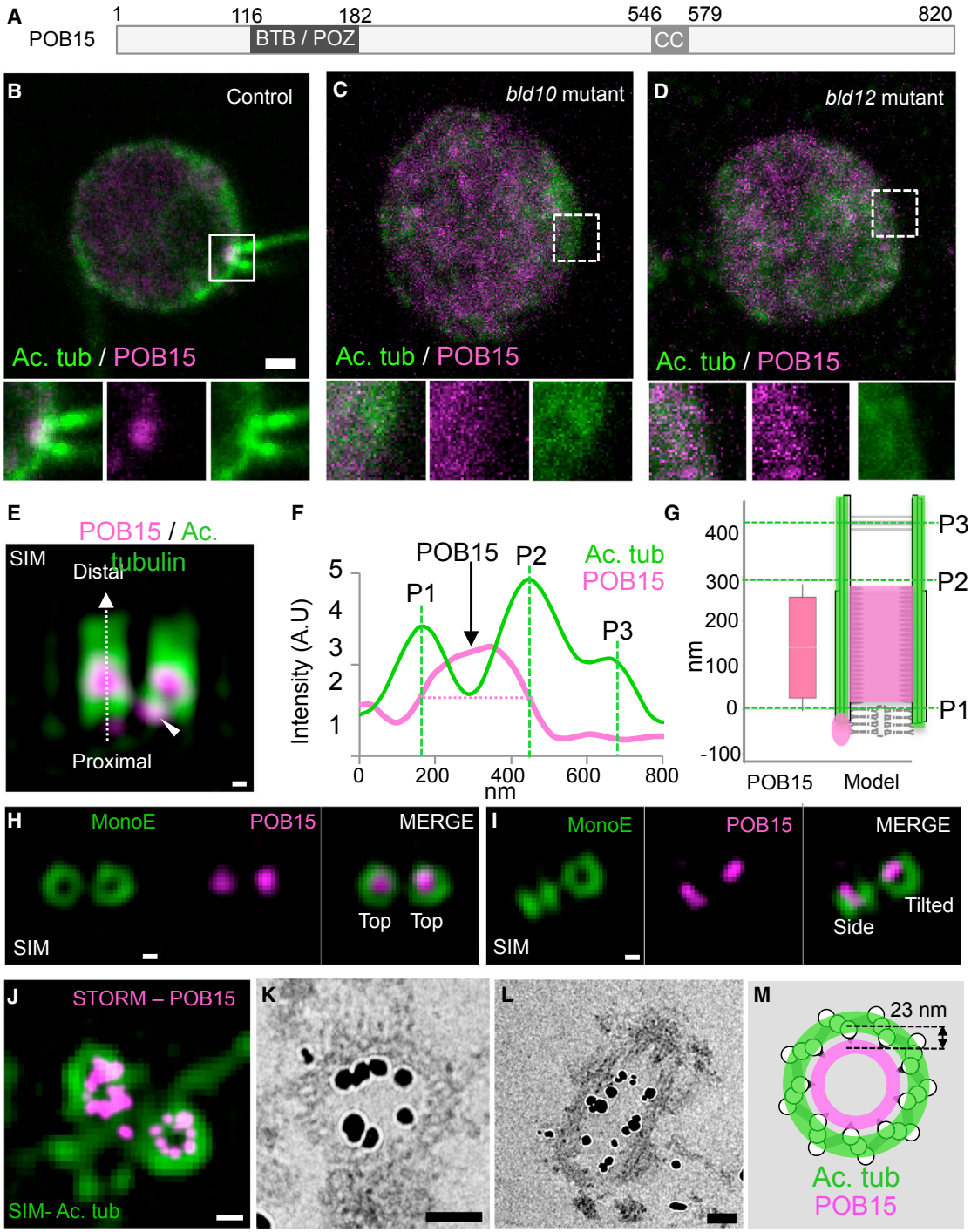


**Figure 4. POB15 Is a *Chlamydomonas* Central Core Protein**

(A) Schematic representation of the 820-amino-acid-long POB15 protein highlighting its predicted BTB/POZ and coiled coil (CC) domains.

(B–D) Immunofluorescence microscopy of *Chlamydomonas* control (B), *bld10* null mutant (C), and *bld12* null mutant (D) cells stained with antibodies against acetylated tubulin (green) and POB15 (magenta). Here and in other figures, insets are 2-fold magnified views of the region indicated in the lower magnification views, with dashed contours indicating those mutant cases in which centrioles are lacking, shown for visualization purposes, as it is not possible to ascertain where exactly below the plasma membrane centrioles would have been. The scale bar represents 1 μm.

(E) SIM image of purified *Chlamydomonas* centrioles viewed from the side and stained with antibodies against acetylated tubulin (green) and POB15 (magenta). Note the central core localization of the bulk of POB15, as well as the proximal focus (arrowhead). The scale bars represent 100 nm.

(F) Superimposed plot profiles of acetylated tubulin (green) and POB15 (magenta).

(G) Schematic representation of POB15 localization (height: 229 ± 29 nm; magenta) as compared to that of acetylated tubulin (green). Data are represented as mean ± SD.

*(legend continued on next page)*

database termed POBdb (Figure 3D; http://pobdb.vital-it.ch/). POBdb provides extensive information regarding each protein identified in the present analysis, including those not retained among the 65 candidates. This includes the actual peptides identified by mass spectrometry, as well as co-expression data for the corresponding genes from the *Chlamydomonas* database Phytozome (https://phytozome.jgi.doe.gov). Moreover, homologs of proteins uncovered here and that were previously identified in centrosome/basal body mass spectrometric analyses in human cells, *Drosophila melanogaster* and *Tetrahymena thermophila*, are highlighted. Furthermore, users can interrogate and rank the proteomic data using several criteria, as well as BLAST a protein of interest from any species against the proteomic dataset within POBdb. Overall, we expect POBdb to be a valuable tool for the scientific community interested in centriole and cilia biology.

## Identification and Localization of the Central Core Component POB15

We focused further analysis on the previously uncharacterized candidate centriolar protein POB15. POB15 is 820 amino acids long and contains a BTB/POZ domain in its N terminus, which is important for protein/protein interactions in other contexts [34], as well as a small predicted coiled-coil in the C-terminal half (Figure 4A).

To ascertain whether POB15 is a bona fide centriolar protein, we raised and affinity purified polyclonal antibodies against a fragment of the protein, which recognized a band at the expected size of ~90 kDa in centriolar extracts (Figures S3A–S3C). Immunofluorescence analysis of wild-type *Chlamydomonas* cells co-stained for acetylated tubulin and POB15 demonstrated that POB15 localizes primarily at centrioles (Figure 4B). In an attempt to assess the specificity of the POB15 signal and explore the function of the corresponding protein, we analyzed the only available potential *pob15* mutant strain generated by the Chlamy Library project (https://www.chlamylibrary.org/) [35]. However, PCR analysis revealed that this strain did not contain an insertion in the *pob15* genomic region (data not shown). We assessed whether the focused POB15 signal depended on the presence of centrioles by conducting immunofluorescence analysis on *bld10* mutant cells, which lack the organelle [16, 30]. Importantly, we found that no focused POB15 signal was detected in this case, indicating that POB15 specifically localizes to centrioles in vivo (Figures 4C, S4A, and S4B).

We next investigated the precise distribution of POB15 at centrioles using SIM imaging. Strikingly, we found that POB15 localizes primarily to an ~250-nm-long region between P1 and P2, as well as to a small focus just below the proximal end (Figures 4E–4G). Moreover, we found that POB15 colocalizes with the central core marker MonoE (Figures 4H and 4I). To further test whether POB15 localizes elsewhere than on the cartwheel-bearing region of centrioles, we made use of *Crsas-6* null mutants, because ~15% of *Chlamydomonas* cells lacking *Crsas-6* nevertheless form centrioles, which are devoid of cartwheel [16]. Importantly, we found that, whereas no focus of POB15 was detected in ~83% of *Crsas-6* cells, ~17% of them retained such a focus (Figures 4D and S4C). This result demonstrates that POB15 does not localize to the cartwheel but is present in centrioles built without that structure.

We next investigated the precise localization of POB15 within the central core region to determine whether it is present in the luminal part or instead is coincident with the Y-shaped linker on the inner barrel adjacent to the microtubule wall [5]. To distinguish between these possibilities, we performed correlative SIM/STORM (stochastic optical reconstruction microscopy) super-resolution microscopy to precisely map POB15 distribution [19]. Using acetylated tubulin as a spatial reference, we found that POB15 localizes close to the inner side of the microtubule wall within the central core region (Figure 4J). This localization was confirmed using immuno-electron microscopy, which revealed decoration of gold beads on average ~23 nm away from the inner microtubule wall (Figures 4K–4M). Taking into account that primary and secondary antibodies together are ~20 nm long, this suggests that POB15 localizes very close to the inner surface of centriolar microtubules, seemingly overlapping with the inner barrel comprising the Y-shaped linker structure.

In summary, through mass-spectrometry-based discovery coupled to super-resolution microscopy precision mapping, we identified POB15 as an inner barrel protein localizing to the central core region of the centriole.

## POB15 Is Recruited during Centriole Elongation

To gain insight into when during the assembly process POB15 is incorporated into the nascent procentriole, we designed an assay in which the entire population of procentrioles is analyzed for the presence of given pairs of proteins to infer their relative order of recruitment. We first analyzed in this manner the distribution of the cartwheel protein CrSAS-6 relative to acetylated tubulin (Figures 5A–5C). We found that, of all procentrioles containing CrSAS-6, ~93% were positive for acetylated tubulin. Conversely, all procentrioles containing acetylated tubulin were also positive for CrSAS-6 (Figure 5C). Therefore, CrSAS-6 is present before acetylated tubulin on the emerging procentriole. We next analyzed CrSAS-6 relative to MonoE (Figures 5D–5F). In this case, of all procentrioles containing CrSAS-6, only ~16% were also positive for MonoE. Conversely, all procentrioles containing MonoE were positive for CrSAS-6 (Figure 5F). We conclude that monoglutamylation of tubulin occurs after CrSAS-6 recruitment, as previously observed in another green alga, *Spermatozopsis similis* [36].

We applied a similar reasoning to place POB15 in the sequence of events leading to organelle assembly. We thus discovered that, of all procentrioles containing acetylated

(H and I) SIM images of centrioles stained with MonoE (green) and POB15 (magenta). The scale bars represent 100 nm.

(J) Top view of centrioles imaged using dual SIM/STORM microscopy. Images corresponding to acetylated tubulin (green, SIM) and POB15 (magenta, STORM) were superimposed. The scale bar represents 100 nm.

(K–M) Immuno-EM of isolated *Chlamydomonas* centrioles (K, side view; L, top view), highlighting the localization of POB15 close to the inner microtubule wall and corresponding schematic representation of gold bead distribution (M); average distance from the center of gold beads to the center of the inner-most microtubule: 23.5 ± 4.5 nm. The scale bars represent 100 nm. Data are represented as mean ± SD.

See also Figures S3 and S4.

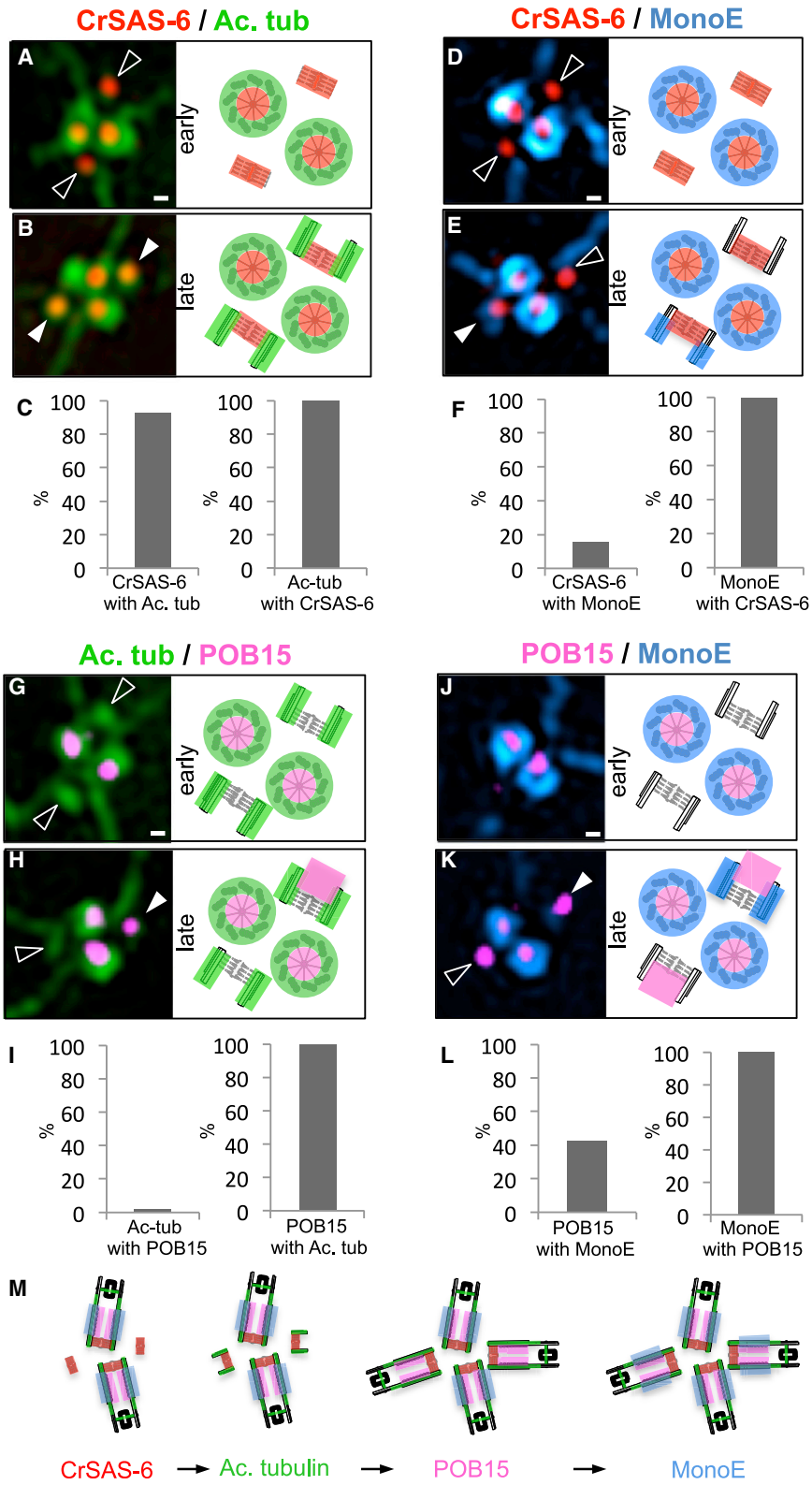


**Figure 5. The Central Core Protein POB15 Is Recruited during Centriole Elongation**

(A, B, D, E, G, H, J, and K) SIM images of isolated centrioles stained with either CrSAS-6 and acetylated tubulin (A and B), CrSAS-6 and MonoE (D and E), acetylated tubulin and POB15 (G and H), or POB15 and MonoE (J and K), visible in the colors indicated above the panels, together with corresponding schematic representations on the right. Data from one experiment are shown. The filled arrowheads indicate colocalization of both markers at procentriole; the empty arrowheads indicate procentrioles that are labeled with just one of the two markers. Note that, in some cases, the two procentrioles can be at slightly different stages of the assembly process (as, for instance, in E). The scale bar represents 100 nm.

(C) Percentage of procentrioles marked by CrSAS-6 that are also positive for acetylated tubulin (left) and percentage of procentrioles marked with acetylated tubulin that are also positive for CrSAS-6 (right).

(F) Percentage of procentrioles marked by CrSAS-6 that are also positive for MonoE (left) and percentage of procentrioles marked with MonoE that are also positive for CrSAS-6 (right).

(I) Percentage of procentrioles marked by acetylated tubulin that are also positive for POB15 (left) and percentage of procentrioles marked with POB15 that are also positive for acetylated tubulin (right).

(L) Percentage of procentrioles marked by POB15 that are also positive for MonoE (left) and percentage of procentrioles marked with MonoE that are also positive for POB15 (right).

(M) Schematic representation of centrioles and stages of procentriole assembly, with the corresponding distribution of the indicated centriolar markers.

tubulin, only ~2% were positive for POB15, whereas 98% of procentrioles positive for POB15 also harbored acetylated tubulin (Figures 5G–5I). Moreover, all procentrioles harboring MonoE were also positive for POB15, whereas only ~43% of procentrioles harboring POB15 were also marked with MonoE (Figures 5J–5L). Taken together, these findings indicate that POB15 is recruited to procentrioles after tubulin acetylation but prior to tubulin monoglutamylation (Figure 5M).

## POC16 Localizes to the Central Core of the Centriole

We became also interested in POC16, a protein highly enriched in centrioles both in the present mass spectrometry dataset and in the earlier proteomic work (Table S2) [8] but whose distribution at centrioles had not been investigated. POC16 is an evolutionarily conserved protein of 2,083 amino acids that comprises a DUF667 domain (domain of unknown function) in its N terminus, followed by multiple WD40 repeats (Figures 6A and S6). Of particular interest, DUF667 is also present in the *Chlamydomonas*

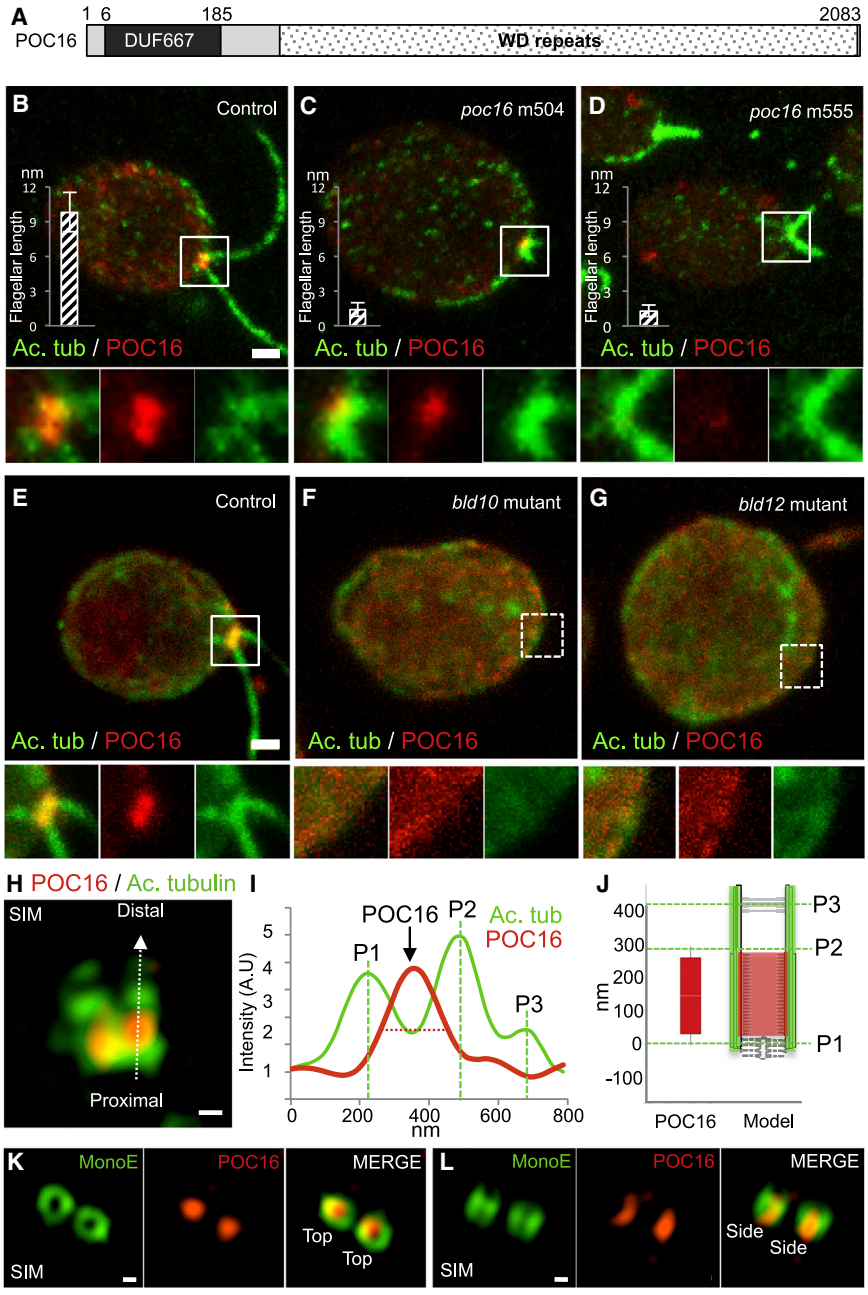


**Figure 6. POC16 Is a Central Core Protein**

(A) Schematic representation of the 2,083-amino-acid-long centriolar protein POC16, with its DUF667 (domain of unknown function) domain and WD40 repeats.

(B–G) Confocal images of *Chlamydomonas* control (B and E), two *poc16* mutants (C and D), *bld10* null mutant (F), and *bld12* null mutant (G) cells stained for POC16 (red) and acetylated tubulin (green). Note the striking reduction of POC16 signal in the *poc16* mutant strains, as well as shorter flagella in both mutants as reported in the bar graphs within (B)–(D). (B–D) Averages and SEs are indicated: 9.8 ± 1.7 (wild-type); 1.4 ± 0.6 (m504); and 1 ± 0.6 (m555). The scale bar represents 1 μm.

(H) SIM image of purified centrioles stained with antibodies against acetylated tubulin (green) and POC16 (red). The scale bar represents 100 nm.

(I) Superimposed plot profiles of acetylated tubulin (green) and POC16 (red).

(J) Schematic representation of POC16 (228 ± 33 nm; red) as compared to that of acetylated tubulin (green) together. Error bars represent SD.

(K and L) SIM images of centrioles stained with MonoE (green) and POC16 (red). The scale bars represent 100 nm.

See also Figures S3–S5 and Movie S1.

ciliary protein FAP20 (flagellar-associated protein 20), which is an inner junction protein of axonemal doublet microtubules [37]. By extension, it has been proposed that POC16 may be part of the Y-shaped linker in the centriole and thus promote the joining of A and B microtubules [37].

We sought to determine the localization of POC16 at centrioles by raising and affinity purifying antibodies against a fragment of POC16. Although these antibodies recognized the recombinant protein in western blot, they did not detect the ~230-kDa protein in centriolar extracts, perhaps reflecting epitope masking or low protein levels in vivo (Figures S3D and S3F). Regardless, immunofluorescence analysis of wild-type *Chlamydomonas* cells uncovered a signal at centrioles (Figure 6B). To ascertain the specificity of this signal, we analyzed the distribution of POC16 in putative *poc16* mutants even through they are not necessarily expected to be null alleles [35]. Thus, five *poc16* putative mutants generated by the Chlamy Library project [35] were analyzed by PCR, which verified the insertion of a 2.2-kb CIB1 cassette in the *poc16* genomic region in all five cases (Figures S5A–S5F). Importantly, immunofluorescence analysis uncovered a clear reduction of the centriolar signal in several of these strains, indicating that POC16 localizes at centrioles in *Chlamydomonas* cells (Figures 6B–6D and S5G–S5J). Compatible with this view, no focused signal was detected in *bld10* mutant cells (Figures 6E–6G, S4D, and S4E). Moreover, like for POB15, we found that a focused POC16 signal is missing from ~83% *bld12* mutant cells but can be detected in the remaining ~17%, indicating that POC16 localizes to centrioles that are devoid of cartwheel (Figures 6G and S4F). Furthermore, we found that POB15 centriolar localization is not affected in *poc16* mutant cells, suggesting that POB15 localization at centrioles is independent of POC16 function (Figures S5M–S5S).

We next assessed the precise localization of POC16 using SIM (Figure 6H). Importantly, we found that, just like POB15, POC16 localizes to a region ~230 nm in length located between P1 and P2, corresponding to the central core region (Figures 6I and 6J). Furthermore, we found that POC16 localizes within the microtubule wall marked with MonoE (Figures 6K and 6L). Overall,

we conclude that POC16 is another constituent of the central core region of *Chlamydomonas* centrioles.

We then wanted to investigate the function of this novel central core protein. To do so, we took advantage of the characterized *poc16* mutants. Interestingly, we found that two of the *poc16* mutants exhibited shorter flagella defects and were not able to swim (Figures 6B–6D, bar graphs, and S5L; Movie S1). The fact that not all *poc16* mutants displayed such a phenotype may be due to the fact that they are not null alleles. Regardless, these results taken together indicate that POC16 is somehow important for flagellum assembly and/or maintenance.

## WDR90 Is a Positive Regulator of Ciliogenesis in Human Cells

In a further attempt to investigate the function of central core region components, we turned to cultured human cells. Whereas there appears to be no human protein homologous to POB15, the protein WDR90 is the human ortholog of POC16 (Figure S6). WDR90 has been detected in several proteomic analyses of centrosomes [11], but its function has not been tested to date.

We first determined the subcellular distribution of WDR90 in RPE-1 ciliated human retinal-pigmented epithelial cells. We found that antibodies against WDR90 decorated both mother and daughter centrioles, and this in a specific manner, because the centriolar signals diminished greatly upon WDR90 depletion by small interfering RNA (siRNA) (Figures 7A, S7D, and S7E). Although the signal-to-noise ratio of these antibodies made them unsuitable for analysis by SIM, we assessed WDR90 localization in more detail using confocal microscopy, comparing its position to MonoE. In human cells, the center of the region carrying this post-translational modification is located ~280 nm from the distal tip marker CP110, thus more proximally than in *Chlamydomonas* (Figures 7B and 7E) [38]. Importantly, we found that the center of the WDR90 signal lies ~180 nm away from that of the MonoE signal and a mere ~60 nm away from the center of the signal for the distal luminal marker centrin (Figures 7C–7E). We conclude that WDR90 and Centrin nearly co-localize in the distal part of human centrioles. Because a structure reminiscent of the Y-shaped linker has been observed in the distal region of purified human centrioles [6, 7], and because Centrin, a distal marker in human centriole, localizes in the central core region in *Chlamydomonas* [39], we propose that the central core region of the *Chlamydomonas* centriole is related to the distal region of the human centriole and that POC16/WDR90 localizes similarly to these two regions.

We next assessed the impact on centriole duplication of depleting WDR90 from cycling U2OS cells by counting the number of Centrin foci present during mitosis. Most control cells have four such foci, and we found no statistical difference from this situation in cells depleted of WDR90 (Figures S7A–S7C). We conclude that WDR90 is not necessary for centriole assembly.

We next investigated whether WDR90 is required for ciliogenesis in serum-starved RPE-1 p53$^{-}$ cells by following the ciliary marker BBS4. Importantly, we found that, whereas ~68% of control cells harbored a primary cilium, this was the case of only ~32% of cells treated with siRNAs targeting WDR90 (Figures 7F–7H). Likewise, using the ciliary marker MonoE, we found that, whereas ~60% of cells transfected with control siRNA displayed cilia, this was the case of only ~27% of cells treated with siRNAs targeting WDR90 (Figures 7I–7L). To verify that this phenotype corresponds to an on-target effect, we generated a cell line stably expressing a siRNA-resistant version of WDR90 fused to GFP and driven by a doxycycline-inducible promoter. Expression of this construct significantly rescued the ciliary defect as assessed by MonoE staining, with ~50% of cells harboring cilia (Figures 7I–7L), indicating that the observed defects in ciliogenesis are due, at least to a large extent, to depletion of WDR90.

In order to explore the root of the ciliogenesis defect, we tested whether the capping protein CP110 was correctly removed [40] in WDR90-depleted cells and found this to be the case (Figure S7F), indicating that lack of CP110 removal cannot explain the observed ciliogenesis defect. The recruitment of the transition zone proteins Cep290 [41] and TCTN1 [42] was also not affected, suggesting that at least part of the transition zone forms correctly in WDR90-depleted cells (Figures S7G and S7H). Likewise, the distribution of Cep164, which is required for docking of the centriole below the plasma membrane [43], was not altered either (Figure S7I). Overall, we conclude that the initial steps of ciliogenesis are executed correctly in WDR90-depleted cells, indicating that WDR90 is required at a later stage for efficient primary cilium formation in human cells.

## DISCUSSION

Centrioles are large macromolecular assemblies constituted by well over 100 different proteins present in many copies within the centriole [14]. Correlating the centriolar architecture, including sub-ultrastructural assemblies, with protein composition is a major challenge that needs to be tackled to fully understand centriole biogenesis and function.

In this work, we undertook a semiquantitative proteomic analysis of isolated *Chlamydomonas* centrioles to identify novel centriolar components. We then used super-resolution microscopy to unveil the precise spatial distribution within the centriole of two select proteins. We thus discovered that POB15 and POC16 localize to the central core region of *Chlamydomonas* centrioles. More precisely, we demonstrated that POB15 localizes next to centriolar microtubules within the central core, a region known to harbor the Y-shaped linker in *Chlamydomonas* [5]. POC16, through its analogy to FAP20, has been proposed to be part of this structure [37], and we provide here the first experimental evidence supporting this hypothesis. More generally, our work complements previous proteomic analysis of *Chlamydomonas* centrioles [15] and provides a rich starting point for the spatial mapping of multiple proteins within the centriole, with the ultimate goal of linking these with ultrastructural features and functional attributes.

The function of POB15 could not be addressed because no proper *Chlamydomonas* mutant is available for the corresponding gene, and reverse genetics has been challenging in this organism. Moreover, we could not identify a human homolog of POB15, precluding us from undertaking functional analysis in that system. By contrast, POC16 has a clear human homolog in WDR90. Interestingly, WDR90 is located in human centrioles essentially coincident with the distal luminal marker Centrin.

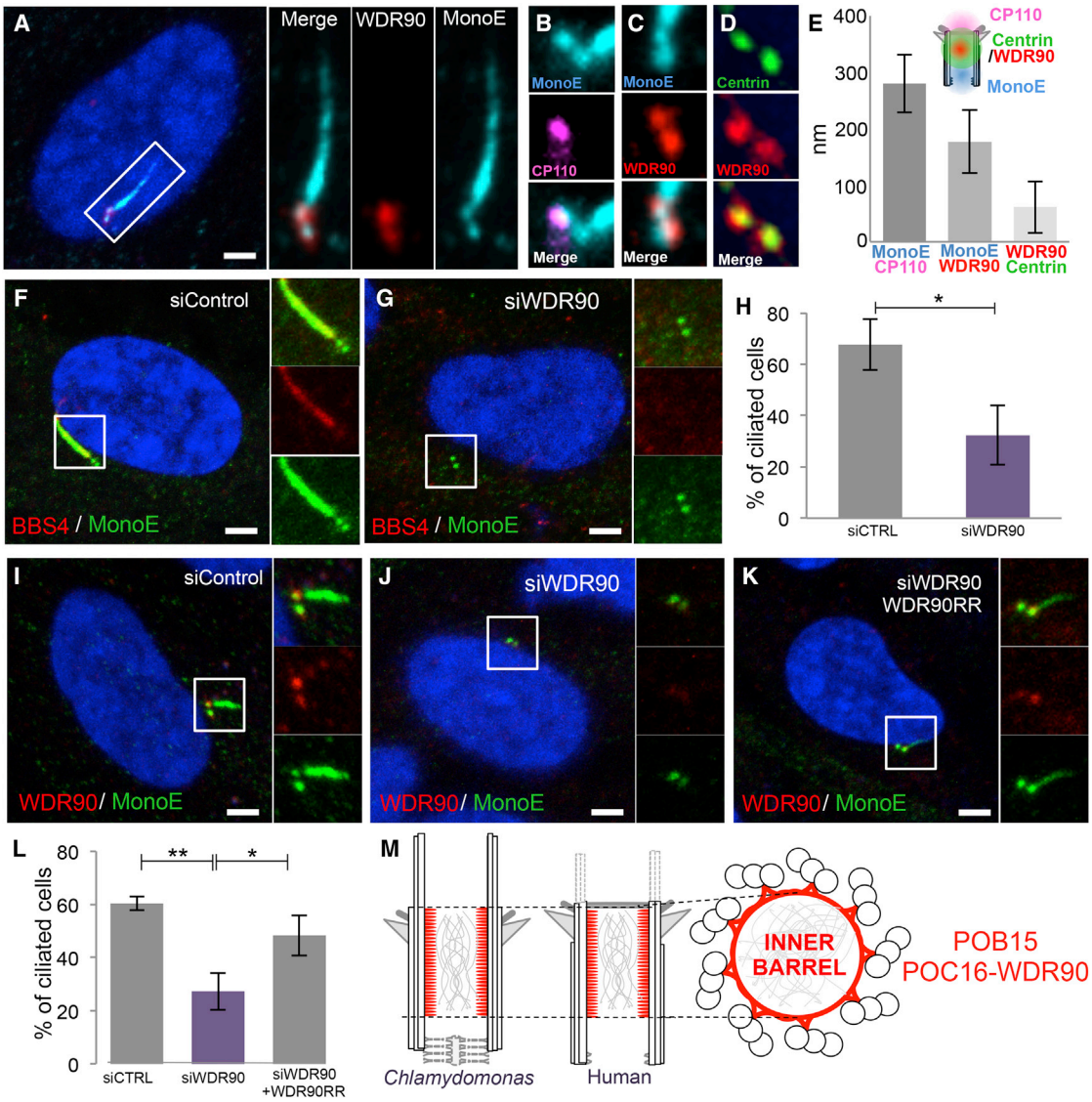


**Figure 7. The POC16 Human Homolog WDR90 Is Required for Ciliogenesis**

(A) Confocal images of RPE-1 p53$^{-}$ cells after induction of ciliogenesis, stained for MonoE (cyan) and WDR90 (red); DNA is visible in blue throughout this figure. Note that WDR90 marks both mother and daughter centrioles. The scale bar represents 2 μm, and all panels are at the same magnification.

(B–D) Insets of human centrioles from RPE-1 p53$^{-}$ cells stained with antibodies against MonoE (cyan) and CP110 (magenta) (B), MonoE (cyan) and WDR90 (red) (C), or Centrin (green) and WDR90 (red) (D), as indicated.

(E) Distances from the centers of the CP110 signal to the MonoE signal (280 ± 52 nm), as well as from the WDR90 signal to the MonoE signal (177 ± 56 nm) or to the Centrin signal (61 ± 46 nm). Schematic representation of the results is shown in the upper inset. Data are represented as mean ± SD.

(F and G) Confocal images of RPE-1 p53$^{-}$ cells transfected with control siRNAs (F) or with siRNAs targeting WDR90 (G), serum-starved for 48 hr to induce ciliogenesis and then analyzed by immunofluorescence against BBS4 (red) and MonoE (green). The scale bar represents 2 μm.

(H) Percentage of RPE-1 p53$^{-}$ cells harboring a primary cilium in the indicated conditions 48 hr after serum starvation. Average for control ± SD: 68% ± 10%; siWDR90: 32% ± 11%. Student two-tailed t tests are as follows: control/siWDR90; p = 0.01608.

(I and J) Confocal images of RPE-1 p53$^{-}$ cells transfected with control siRNAs (I) or siRNAs targeting WDR90 (J), serum starved for 48 hr to induce ciliogenesis, and then analyzed by immunofluorescence against WDR90 (red) and MonoE (green). The scale bars represent 2 μm.

(K) Confocal images of RPE-1 p53$^{-}$ cells transfected with siRNAs targeting WDR90, induced by doxycycline to express RNAi-resistant WDR90, serum starved for 48 hr to induce ciliogenesis, and then analyzed by immunofluorescence against WDR90 (red) and MonoE (green). The scale bar represents 2 μm.

(L) Percentage of RPE-1 p53$^{-}$ cells harboring a primary cilium in the indicated conditions 48 hr after serum starvation. Average for control ± SD: 62% ± 5%; siWDR90: 27% ± 7%; siWDR90+WDR90RR: 48% ± 7%. Student two-tailed t tests are as follows: control/siWDR90, p = 0.00241; siWDR90/siWDR90+WDR90RR, p = 0.02441.

(M) Schematic representation of *Chlamydomonas* and human centrioles, highlighting the central core region (red) located in the middle of the *Chlamydomonas* centriole—hence its name—and in the human centriole. POB15 and POC16/WDR90 both reside in the inner barrel within these regions.

See also Figures S6 and S7.

We propose that this region of human centrioles corresponds to the central core region of *Chlamydomonas* centrioles, which also harbors Centrin [39] (Figure 7M).

The Y-shaped linker has been hypothesized to be important for microtubule stabilization within the centriole [5]. Importantly, we found that in both *Chlamydomonas* and human cells, impairing POC16 or WDR90 function leads to flagellar or ciliary defects, suggesting that the inner barrel coincident with the Y-shaped linker somehow promotes flagellum and cilium formation. Perhaps POC16 and WDR90 strengthen the Y-shaped linker and, consequently, the surrounding microtubules wall, thereby ensuring proper flagellum or cilium assembly. An alternative hypothesis is that trafficking toward the ciliary compartment goes through the centriole lumen and is somewhat regulated by the Y-shaped linker and associated proteins, such as POC16 and WDR90. Whether the Y-shaped linker is present in other systems is not known at present, but the good overall conservation of POC16 proteins (Figure S6) raises the possibility that this may be the case. In addition, other components that have been localized in the vicinity of microtubule triplets in *Tetrahymena* and *Trypanosoma* [9, 44] could also be part of the Y-shaped linker. Further studies using high-resolution mapping, including STORM microscopy and immuno-EM, should provide a comprehensive molecular mapping of the proteins composing the inner barrel of centrioles.

Another important discovery of this study stems from the fact that mono- and poly-glutamylation post-translation modifications of tubulin specifically decorate the central core region of *Chlamydomonas* centrioles. This implies that a spatial code exists along the proximal-distal axis of centrioles, which may lead to the recruitment of specific proteins within distinct centriolar regions. Deciphering such a spatial code might have bearing on understanding overall centriole architecture and function.

## STAR★METHODS

Detailed methods are provided in the online version of this paper and include the following:



## SUPPLEMENTAL INFORMATION

Supplemental Information includes seven figures, two tables, and one movie and can be found with this article online at http://dx.doi.org/10.1016/j.cub.2017.07.011.

## AUTHOR CONTRIBUTIONS

V.H. and P. Guichard designed, performed, and analyzed all the experiments of the paper and wrote the manuscript. E.S. performed and analyzed the data in Figures 7 and S7D–S7I. R.H. and F.A. performed the mass spectrometry analysis. I.F. purified GST-POB15 and GST-POC16 proteins. C.B. performed the experiment shown in Figures S7A and S7B. N.O. and M.O.S. produced the cleaved POC16 protein. S.B. performed the western blots in Figure S3 and the immunofluorescence analysis in Figures 6B–6D, S5G–S5J, and S5M–S5S, as well as performed the mapping of the *Chlamydomonas* mutants by PCR (Figures S5A–S5F). C.O.S.S. performed with P. Guichard the single particle analysis reconstruction shown in Figure 1F. P. Gönczy analyzed and supervised the work, as well as wrote the manuscript.

## ACKNOWLEDGMENTS

We thank Alexandra Bezler, George Haztopoulos, and Michel Goldschmidt-Clermont for critical reading of the manuscript. We are grateful to Mathias Fournier (BiOP core facility, School of Life Sciences, EPFL) for help with SIM/STORM acquisition, Maeva LeGuennec for help with Figure 2, Meng-Fu Bryan Tsou for the gift of RPE-1 p53$^{-}$ cells, and Masafumi Hirono for the gift of Bld10p antibodies. P. Guichard and V.H. are currently supported by the Swiss National Science Foundation (SNSF) PP00P3_157517 and E.S. and S.B. by the University of Geneva. This work was supported by grant AdG 340227 from the European Research Council to P. Gönczy, which funded P. Guichard, V.H., and I.F.

Received: February 23, 2017
Revised: June 8, 2017
Accepted: July 4, 2017
Published: August 3, 2017

## REFERENCES


1. Conduit, P.T., Wainman, A., and Raff, J.W. (2015). Centrosome function and assembly in animal cells. Nat. Rev. Mol. Cell Biol. *16*, 611–624.
2. Bornens, M. (2012). The centrosome in cells and organisms. Science *335*, 422–426.
3. Gönczy, P. (2012). Towards a molecular architecture of centriole assembly. Nat. Rev. Mol. Cell Biol. *13*, 425–435.
4. Winey, M., and O'Toole, E. (2014). Centriole structure. Philos. Trans. R. Soc. Lond. B Biol. Sci. *369*, 20130457.
5. Li, S., Fernandez, J.J., Marshall, W.F., and Agard, D.A. (2012). Three-dimensional structure of basal body triplet revealed by electron cryo-tomography. EMBO J. *31*, 552–562.
6. Hilbert, M., Noga, A., Frey, D., Hamel, V., Guichard, P., Kraatz, S.H., Pfreundschuh, M., Hosner, S., Flückiger, I., Jaussi, R., et al. (2016). SAS-6 engineering reveals interdependence between cartwheel and microtubules in determining centriole architecture. Nat. Cell Biol. *18*, 393–403.
7. Vorobjev, I.A., and Chentsov, Y.S. (1980). The ultrastructure of centriole in mammalian tissue culture cells. Cell Biol. Int. Rep. *4*, 1037–1044.
8. Keller, L.C., Romijn, E.P., Zamora, I., Yates, J.R., 3rd, and Marshall, W.F. (2005). Proteomic analysis of isolated Chlamydomonas centrioles reveals orthologs of ciliary-disease genes. Curr. Biol. *15*, 1090–1098.

9. Kilburn, C.L., Pearson, C.G., Romijn, E.P., Meehl, J.B., Giddings, T.H., Jr., Culver, B.P., Yates, J.R., 3rd, and Winey, M. (2007). New Tetrahymena basal body protein components identify basal body domain structure. J. Cell Biol. *178*, 905–912.
10. Andersen, J.S., Wilkinson, C.J., Mayor, T., Mortensen, P., Nigg, E.A., and Mann, M. (2003). Proteomic characterization of the human centrosome by protein correlation profiling. Nature *426*, 570–574.
11. Jakobsen, L., Vanselow, K., Skogs, M., Toyoda, Y., Lundberg, E., Poser, I., Falkenby, L.G., Bennetzen, M., Westendorf, J., Nigg, E.A., et al. (2011). Novel asymmetrically localizing components of human centrosomes identified by complementary proteomics methods. EMBO J. *30*, 1520–1535.
12. Firat-Karalar, E.N., and Stearns, T. (2015). Probing mammalian centrosome structure using BioID proximity-dependent biotinylation. Methods Cell Biol. *129*, 153–170.
13. Müller, H., Schmidt, D., Steinbrink, S., Mirgorodskaya, E., Lehmann, V., Habermann, K., Dreher, F., Gustavsson, N., Kessler, T., Lehrach, H., et al. (2010). Proteomic and functional analysis of the mitotic Drosophila centrosome. EMBO J. *29*, 3344–3357.
14. Bauer, M., Cubizolles, F., Schmidt, A., and Nigg, E.A. (2016). Quantitative analysis of human centrosome architecture by targeted proteomics and fluorescence imaging. EMBO J. *35*, 2152–2166.
15. Keller, L.C., and Marshall, W.F. (2008). Isolation and proteomic analysis of Chlamydomonas centrioles. Methods Mol. Biol. *432*, 289–300.
16. Nakazawa, Y., Hiraki, M., Kamiya, R., and Hirono, M. (2007). SAS-6 is a cartwheel protein that establishes the 9-fold symmetry of the centriole. Curr. Biol. *17*, 2169–2174.
17. Merchant, S.S., Prochnik, S.E., Vallon, O., Harris, E.H., Karpowicz, S.J., Witman, G.B., Terry, A., Salamov, A., Fritz-Laylin, L.K., Maréchal-Drouard, L., et al. (2007). The Chlamydomonas genome reveals the evolution of key animal and plant functions. Science *318*, 245–250.
18. Jost, A., and Heintzmann, R. (2013). Superresolution multidimensional imaging with structured illumination microscopy. Annu. Rev. Mater. Res. *43*, 261–282.
19. Hamel, V., Guichard, P., Fournier, M., Guiet, R., Flückiger, I., Seitz, A., and Gönczy, P. (2014). Correlative multicolor 3D SIM and STORM microscopy. Biomed. Opt. Express *5*, 3326–3336.
20. Janke, C., and Bulinski, J.C. (2011). Post-translational regulation of the microtubule cytoskeleton: mechanisms and functions. Nat. Rev. Mol. Cell Biol. *12*, 773–786.
21. Hiraki, M., Nakazawa, Y., Kamiya, R., and Hirono, M. (2007). Bld10p constitutes the cartwheel-spoke tip and stabilizes the 9-fold symmetry of the centriole. Curr. Biol. *17*, 1778–1783.
22. Guichard, P., Hamel, V., Le Guennec, M., Banterle, N., Iacovache, I., Nemčíková, V., Flückiger, I., Goldie, K.N., Stahlberg, H., Lévy, D., et al. (2017). Cell-free reconstitution reveals centriole cartwheel assembly mechanisms. Nat. Commun. *8*, 14813.
23. Guichard, P., Hachet, V., Majubu, N., Neves, A., Demurtas, D., Olieric, N., Fluckiger, I., Yamada, A., Kihara, K., Nishida, Y., et al. (2013). Native architecture of the centriole proximal region reveals features underlying its 9-fold radial symmetry. Curr. Biol. *23*, 1620–1628.
24. Kovanich, D., Cappadona, S., Raijmakers, R., Mohammed, S., Scholten, A., and Heck, A.J.R. (2012). Applications of stable isotope dimethyl labeling in quantitative proteomics. Anal. Bioanal. Chem. *404*, 991–1009.
25. Cox, J., and Mann, M. (2008). MaxQuant enables high peptide identification rates, individualized p.p.b.-range mass accuracies and proteome-wide protein quantification. Nat. Biotechnol. *26*, 1367–1372.
26. Chopra, T., Hamelin, R., Armand, F., Chiappe, D., Moniatte, M., and McKinney, J.D. (2014). Quantitative mass spectrometry reveals plasticity of metabolic networks in Mycobacterium smegmatis. Mol. Cell. Proteomics *13*, 3014–3028.
27. Kuhn, M., Hyman, A.A., and Beyer, A. (2014). Coiled-coil proteins facilitated the functional expansion of the centrosome. PLoS Comput. Biol. *10*, e1003657.
28. Pfannenschmid, F., Wimmer, V.C., Rios, R.-M., Geimer, S., Kröckel, U., Leiherer, A., Haller, K., Nemcová, Y., and Mages, W. (2003). Chlamydomonas DIP13 and human NA14: a new class of proteins associated with microtubule structures is involved in cell division. J. Cell Sci. *116*, 1449–1462.
29. Weber, K., Geisler, N., Plessmann, U., Bremerich, A., Lechtreck, K.F., and Melkonian, M. (1993). SF-assemblin, the structural protein of the 2-nm filaments from striated microtubule associated fibers of algal flagellar roots, forms a segmented coiled coil. J. Cell Biol. *121*, 837–845.
30. Matsuura, K., Lefebvre, P.A., Kamiya, R., and Hirono, M. (2004). Bld10p, a novel protein essential for basal body assembly in Chlamydomonas: localization to the cartwheel, the first ninefold symmetrical structure appearing during assembly. J. Cell Biol. *165*, 663–671.
31. Nojima, D., Linck, R.W., and Egelman, E.H. (1995). At least one of the protofilaments in flagellar microtubules is not composed of tubulin. Curr. Biol. *5*, 158–167.
32. Singla, V., Romaguera-Ros, M., Garcia-Verdugo, J.M., and Reiter, J.F. (2010). Ofd1, a human disease gene, regulates the length and distal structure of centrioles. Dev. Cell *18*, 410–424.
33. Nogales-Cadenas, R., Abascal, F., Díez-Pérez, J., Carazo, J.M., and Pascual-Montano, A. (2009). CentrosomeDB: a human centrosomal proteins database. Nucleic Acids Res. *37*, D175–D180.
34. Chaharbakhshi, E., and Jemc, J.C. (2016). Broad-complex, tramtrack, and bric-à-brac (BTB) proteins: critical regulators of development. Genesis *54*, 505–518.
35. Li, X., Zhang, R., Patena, W., Gang, S.S., Blum, S.R., Ivanova, N., Yue, R., Robertson, J.M., Lefebvre, P.A., Fitz-Gibbon, S.T., et al. (2016). An indexed, mapped mutant library enables reverse genetics studies of biological processes in Chlamydomonas reinhardtii. Plant Cell *28*, 367–387.
36. Lechtreck, K.F., and Bornens, M. (2001). Basal body replication in green algae–when and where does it start? Eur. J. Cell Biol. *80*, 631–641.
37. Yanagisawa, H.A., Mathis, G., Oda, T., Hirono, M., Richey, E.A., Ishikawa, H., Marshall, W.F., Kikkawa, M., and Qin, H. (2014). FAP20 is an inner junction protein of doublet microtubules essential for both the planar asymmetrical waveform and stability of flagella in Chlamydomonas. Mol. Biol. Cell *25*, 1472–1483.
38. Thauvin-Robinet, C., Lee, J.S., Lopez, E., Herranz-Pérez, V., Shida, T., Franco, B., Jego, L., Ye, F., Pasquier, L., Loget, P., et al. (2014). The oral-facial-digital syndrome gene C2CD3 encodes a positive regulator of centriole elongation. Nat. Genet. *46*, 905–911.
39. Geimer, S., and Melkonian, M. (2005). Centrin scaffold in Chlamydomonas reinhardtii revealed by immunoelectron microscopy. Eukaryot. Cell *4*, 1253–1263.
40. Spektor, A., Tsang, W.Y., Khoo, D., and Dynlacht, B.D. (2007). Cep97 and CP110 suppress a cilia assembly program. Cell *130*, 678–690.
41. Tsang, W.Y., Bossard, C., Khanna, H., Peränen, J., Swaroop, A., Malhotra, V., and Dynlacht, B.D. (2008). CP110 suppresses primary cilia formation through its interaction with CEP290, a protein deficient in human ciliary disease. Dev. Cell *15*, 187–197.
42. Garcia-Gonzalo, F.R., Corbit, K.C., Sirerol-Piquer, M.S., Ramaswami, G., Otto, E.A., Noriega, T.R., Seol, A.D., Robinson, J.F., Bennett, C.L., Josifova, D.J., et al. (2011). A transition zone complex regulates mammalian ciliogenesis and ciliary membrane composition. Nat. Genet. *43*, 776–784.
43. Tanos, B.E., Yang, H.-J., Soni, R., Wang, W.-J., Macaluso, F.P., Asara, J.M., and Tsou, M.-F.B. (2013). Centriole distal appendages promote membrane docking, leading to cilia initiation. Genes Dev. *27*, 163–168.
44. Dang, H.Q., Zhou, Q., Rowlett, V.W., Hu, H., Lee, K.J., Margolin, W., and Li, Z. (2017). Proximity interactions among basal body components in Trypanosoma brucei identify novel regulators of basal body biogenesis and inheritance. MBio *8*, 1–15.

45. Wang, W.J., Acehan, D., Kao, C.H., Jane, W.N., Uryu, K., and Tsou, M.F.B. (2015). De novo centriole formation in human cells is error-prone and does not require SAS-6 self-assembly. eLife *4*, 1–13.

46. Habedanck, R., Stierhof, Y.-D., Wilkinson, C.J., and Nigg, E.A. (2005). The Polo kinase Plk4 functions in centriole duplication. Nat. Cell Biol. *7*, 1140–1146.

47. Davies, D.R., and Plaskitt, A. (1971). Genetical and structural analyses of cell-wall formation in Chlamydomonas reinhardi. Genet. Res. *17*, 33–43.

48. Schneider, C.A., Rasband, W.S., and Eliceiri, K.W. (2012). NIH Image to ImageJ: 25 years of image analysis. Nat. Methods *9*, 671–675.

49. Hutner, S.H., Provasoli, L., Schatz, A., and Haskins, C.P. (1950). Some approaches to the study of the role of metals in the metabolism of microorganisms. Proc. Am. Philos. Soc. *94*, 152–170.

50. Abrishami, V., Zaldívar-Peraza, A., de la Rosa-Trevín, J.M., Vargas, J., Otón, J., Marabini, R., Shkolnisky, Y., Carazo, J.M., and Sorzano, C.O.S. (2013). A pattern matching approach to the automatic selection of particles from low-contrast electron micrographs. Bioinformatics *29*, 2460–2468.

51. Sorzano, C.O.S., Bilbao-Castro, J.R., Shkolnisky, Y., Alcorlo, M., Melero, R., Caffarena-Fernández, G., Li, M., Xu, G., Marabini, R., and Carazo, J.M. (2010). A clustering approach to multireference alignment of single-particle projections in electron microscopy. J. Struct. Biol. *171*, 197–206.

52. Kitagawa, D., Vakonakis, I., Olieric, N., Hilbert, M., Keller, D., Olieric, V., Bortfeld, M., Erat, M.C., Flückiger, I., Gönczy, P., and Steinmetz, M.O. (2011). Structural basis of the 9-fold symmetry of centrioles. Cell *144*, 364–375.

## STAR★METHODS

### KEY RESOURCES TABLE

| REAGENT or RESOURCE | SOURCE | IDENTIFIER |
|---|---|---|
| Antibodies | | |
| Rabbit polyclonal anti-CrSAS-6 | Pierre Gönczy [23] | N/A |
| Rabbit polyclonal anti-POB15 | This paper | N/A |
| Rabbit polyclonal anti-POC16 | This paper | N/A |
| Rabbit polyclonal anti-Polyglutamate chain (PolyE) (IN105) | Adipogen | Cat# AG-25B-0030; RRID: AB_2490540 |
| Rabbit polyclonal anti-Bld10 | Masafumi Hirono [26] | N/A |
| Mouse monoclonal anti alpha-tubulin (2D6) | Thermo Fisher Scientific | Cat# MA5-17193; RRID: AB_2538664 |
| Mouse monoclonal anti-apha tubulin (clone DM1A) | Abcam | Cat# ab7291 RRID: AB_2241126 |
| Alpha-Tubulin (clone 11H10) rabbit mAb (Alexa Fluor 647 conjugate) | Cell Signaling Technology | Cat# 5046 |
| Mouse monoclonal anti-acetylated tubulin (clone 6-11B-1) | Thermo Fisher Scientific | Cat# 32-2700; RRID: AB_2533073 |
| Mouse monoclonal anti-Polyglutamylation modification mAb (GT335) (MonoE, this study) | Adipogen | Cat# AG-20B-0020; RRID: AB_2490210 |
| Rabbit polyclonal anti-WDR90 | Novus | NBP2-31888 |
| Rabbit polyclonal anti-CP110 | Proteintech group | Cat# 12780-1-AP; RRID: AB_10638480 |
| Rabbit polyclonal anti-Cep290 | Lubios (Bethyl) | Cat# A301-659A; RRID: AB_1210910 |
| Rabbit polyclonal anti-TCTN1 | Proteintech group | Cat# 15004-1-AP; RRID: AB_10644442 |
| Rabbit polyclonal anti-Cep164 | Proteintech group | Cat# 22227-1-AP; RRID: AB_2651175 |
| Mouse monoclonal anti-Centrin | Merckmillipore | Cat# 04-1624; RRID: AB_10563501 |
| Nanogold-IgG goat anti rabbit IgG | Nanoprobes | #2003 |
| HQ Silver | Nanoprobes | #2012 |
| Bacterial and Virus Strains | | |
| BL21(DE3) OS | Thermo Fisher Scientific | Cat# C600003 |
| Chemicals, Peptides, and Recombinant Proteins | | |
| GST-POB15(541-820) | This paper | N/A |
| GST-POC16(1-295) | This paper | N/A |
| Lipofectamine RNAiMax | Thermo Fisher Scientific | Cat# 13778030 |
| Lipofectamine 3000 | Thermo Fisher Scientific | Cat# L3000001 |
| DNaseI | ROCHE | 10104159001 |
| DMEM high w/glutamax | Thermo Fisher Scientific | 61965059 |
| L-glutathione reduced | Sigma | G6529 |
| Pierce glutathione agarose | Invitrogen | 16100 |
| Critical Commercial Assays | | |
| GST inclusion body solubilisation and renaturation kit | Cell Biolabs | AKR-110 |
| Deposited Data | | |
| Mass spectrometry proteomics data | ProteomeXchange Consortium | PRIDE: PXD005818 |
| Proteome of Basal Body database website | http://pobdb.vital-it.ch/ | N/A |
| Experimental Models: Cell Lines | | |
| RPE-1 p53- | Brian Tsou [45] | N/A |
| U2OS | Eric Nigg [46] | N/A |
| Experimental Models: Organisms/Strains | | |
| LMJ.RY0402.069504 (m504, this paper) | *Chlamydomonas* Resource Center | CLIP strain LMJ.RY0402.069504 |
| LMJ.RY0402.149555 (m555, this paper) | *Chlamydomonas* Resource Center | CLIP strain, LMJ.RY0402.149555 |
| LMJ.RY0402.103263 (m263, this paper) | *Chlamydomonas* Resource Center | CLIP strain, LMJ.RY0402.103263 |

(*Continued on next page*)

| Continued | | |
|---|---|---|
| REAGENT or RESOURCE | SOURCE | IDENTIFIER |
| LMJ.RY0402.254436 (m36, this paper) | *Chlamydomonas* Resource Center | CLIP strain, LMJ.RY0402.254436 |
| LMJ.RY0402.235032 (m32, this paper) | *Chlamydomonas* Resource Center | CLIP strain, LMJ.RY0402.235032 |
| LMJ.RY0402.072161 (pob15 m161, this paper) | *Chlamydomonas* Resource Center | CLIP strain, LMJ.RY0402.072161 |
| cMJ030 (control wild-type WT, this paper) | *Chlamydomonas* Resource Center | CLIP control strain |
| CW15- | Jean-David Rochaix [47] | N/A |
| bld10 mutant | Masafumi Hirono [21] | N/A |
| bld12 mutant | Masafumi Hirono [16] | N/A |
| Oligonucleotides | | |
| a: CAT TGA CAC CTG TGG TGA GG | This paper | N/A |
| b: AGG CGT GTG TTA AAG AGC GT | This paper | N/A |
| c: ACG CTC TTT AAC ACA CGC CT | This paper | N/A |
| d: TAG GGA GTT GGA CCG AGT TG | This paper | N/A |
| e: TGC TTA CAT CAT CCT CGC AG | This paper | N/A |
| f: AAG CCA AAC CCA ACA ATC TG | This paper | N/A |
| g: CTG CTA CGT GGT GGA AGA CA | This paper | N/A |
| h: TTG GTG GTG GTG ATA ACC CT | This paper | N/A |
| Cassette (1): AAC CAA GTC GAC GTG CCT AC | This paper | N/A |
| Cassette (2): GCA CCA ATC ATG TCA AGC CT | This paper | N/A |
| Silencer select pre-designed siRNA s47097 (WDR90): 5′CCAGUGACCUGUGCUUUGAtt3′ | Thermo Fisher Scientific | Cat# 4392420 |
| Silencer Negative control #5 siRNA 5nmol | Thermo Fisher Scientific | Cat# AM4642 |
| Recombinant DNA | | |
| pEBTet-WDR90RR-FL | This paper | N/A |
| pENTR-WDR90RR-FL | This paper | N/A |
| pHY-pob15 | This paper | N/A |
| pGEX-6-P-POB15(541-820aa) | This paper | N/A |
| pGEX-6-P-POC16(1-295aa) | This paper | N/A |
| Software and Algorithms | | |
| ImageJ | https://imagej.net [48] | N/A |
| Other | | |
| Chelex 100-grade resin | BIORAD | Cat#1421253 |
| Platinum SuperFi DNA polymerase | Thermo Fisher Scientific | Cat#12351010 |
| FBS tet- | Brunschwig | P30-3602 |
| 12mm coverlips | Roth | YX03.1 |
| 15mm coverslips | Menzel Glaser | 631-1341 |

## CONTACT FOR REAGENT AND RESOURCE SHARING

Further information and requests for resources and reagents should be directed to and will be fulfilled by the Lead Contact, Pierre Gönczy (pierre.gonczy@epfl.ch).

## EXPERIMENTAL MODEL AND SUBJECT DETAILS

### *Chlamydomonas* strains

The cell wall-less *Chlamydomonas* strain CW15- [47] as well as the six other *Chlamydomonas* strains used in this study were grown in liquid Tris-acetate-phosphate medium (TAP medium containing Trace) at ~22°C or on TAP plates with 1.5% agar [49]. The six *Chlamydomonas* mutants were generated by the CLIP library group [35] and obtained through the *Chlamydomonas* Resource Center (http://www.chlamycollection.org/). The following strains were obtained: LMJ.RY0402.069504 (m504), LMJ.RY0402.149555 (m555), LMJ.RY0402.103263 (m263), LMJ.RY0402.254436 (m36), LMJ.RY0402.235032 (m32) and LMJ.RY0402.072161 (*pob15* m161) and are reported in the Key Resource Table. Briefly, mutants were generated by electroporation of a DNA cassette (CIB1) conferring resistance to paromomycin into the *Chlamydomonas* strain CMJ030 [35]. Upon receipt, each mutant was streaked to single colonies, maintained at room temperature on TAP plates, and the insertion site of the CIB1 cassette verified by PCR.

### Cell lines and Tissue culture

Human cells RPE-1 p53- (gift from Meng-Fu Bryan Tsou, tested negative for mycoplasma [45]) or U2OS cells (gift from Erich Nigg [46]) were grown at 37°C with 5% $CO_2$ in DMEM supplemented with GlutaMAX (Life Technology), 10% tetracycline-negative fetal calf serum (Brunschwig), penicillin and streptomycin (100 μg/ml). To generate the inducible episomal iRPE-1 p53-:WDR90RR-GFP cell line, RPE-1 p53- cells were transfected using Lipofectamine 3000 (Life Technology). Transfected cells were first selected for 10 days with 5 μg/ml puromycin, starting one day after transfection, and then with 20 μg/ml puromycin. Selected cells were then amplified and frozen. For further experiments, iRPE-1 p53-:WDR90RR-GFP cell line was grown in the medium specified above supplemented with 10 μg/ml puromycin.

## METHOD DETAILS

### Isolation of *Chlamydomonas* centrioles

*Chlamydomonas* centrioles were isolated as follows. Briefly, 1 l of CW15- cells were pelleted at 600 g for 10 min in an Eppendorf 5810R centrifuge, washed once with PBS, and resuspended in 5% sucrose, 10mM HEPES pH 7.0. Cells were deflagellated by a pH shock through the addition of acetic acid 0.5M to a final pH comprised between 4.5 and 4.7, and incubated for one minute stirring. KOH 1N was subsequently added to restore pH to 7.0. Cells were centrifuged at 600 g for 10 min in an Eppendorf 5810R centrifuge to remove detached flagella. The pellet was washed twice with PBS prior to being carefully loaded onto 25% sucrose and spun at 600 g at 4°C for 15 min to remove leftover flagella in the supernatant. Next, the pellet was resuspended with 1-2ml of PBS and the lysis buffer (1mM HEPES; 0.5mM $MgCl_2$; 1% NP-40 supplemented with 5000 units of DNase (Roche)) added at once on the resuspended cells, which were then incubated for 1 hr at 4°C. Lysed cells were spun at 600 g for 10 min in a 50ml Falcon in an Eppendorf 5810R centrifuge at 4°C to remove cell debris. Next, the supernatant was collected and loaded onto a 2ml 60% sucrose cushion, and spun at 11 000 g for 30 min at 4°C. The 3 mL cushion interface (2 mL cushion + 1 mL above the cushion) was mixed and pooled, before loading onto a 40%–70% sucrose gradient (40%–50%-70%), and spun at 25 000 g using the SW 32 Ti rotor (Beckman) for 1 hr 15 min at 4°C. Twelve 500 μL fractions were collected and further analyzed by immunofluorescence.

This isolation of *Chlamydomonas* centrioles has been conducted two times and both the centriolar positives fractions and the contaminants fractions were pooled.

### Proteomic analysis

Isolated centrioles and neighboring control fractions were digested in-solution as described [26]. Briefly, proteins were resuspended in 8 M Urea, 20% acetonitrile (ACN), 0.2% RapiGest. Samples were reduced, alkylated and digested using Lys-C and Trypsin. The reaction was stopped by acidification and RapiGest-cleaved by addition of pure Formic Acid (FA) during a final 1 hr incubation at 37°C. Samples were dimethyl-labeled on Stage Tip as described [26]. Isolated centrioles (Pool 1) were labeled with medium dimethyl reactants ($CD_2O$ + $NaBH_3CN$), and the neighboring control fractions (Pool 2) with heavy dimethyl reactants ($^{13}CD_2O$ + $NaBD_3CN$). Once labeled, samples were eluted, mixed in a 1:1 (medium/heavy) ratio and dried by vacuum centrifugation. For LC-MS/MS analysis, resuspended peptides were separated by reverse phase chromatography on a Dionex Ultimate 3000 RSLC nano UPLC system connected in-line with an Orbitrap Q-exactive. Samples were injected in technical triplicates and separated through gradients (235 min) in order to maximize both protein identification and relative quantification accuracy. Raw files were processed in MaxQuant 1.2.2.5 using an in-house database generated by combining *Chlamydomonas* proteins sequences from Phytozome (http://phytozome.jgi.doe.gov - PhytozomeV9: Creihardtii_236), UniProtKB/TrEMBL (Release 2014_05) and common contaminants. A threshold of 1% false discovery rate was fixed at the peptide and protein levels. Carbamidomethylation was set as a fixed modification, and Oxidation (Met), phosphorylation (Ser, Thr, and Tyr) as well as acetylation (protein N terminus) were considered as variable modifications. Protein quantifications were performed with Razor and unique peptides using only unmodified, oxidized (Met), and acetylated (protein N terminus) peptides. A minimum of one ratio count was required for quantification. Graphical displays were generated using homemade programs written in R (http://www.r-project.org). The mass spectrometry proteomics data have been deposited to the ProteomeXchange Consortium via the PRIDE partner repository with the dataset identifier PXD005818.

### Cloning

A codon-optimized version of the *pob15* gene was synthesized by Genecust Europe (Luxembourg) using the *Chlamydomonas* codon usage, and cloned in the pHY vector (Amp resistant; used for expression in *Chlamydomonas*, gift from Masafumi Hirono) using the BamHI (5′) and EcoRI (3′) restriction sites. No stop codon was included owing to the presence of a 3xHA tag at the 3′ end of the construct to generate a C_terminus fusion protein POB15_HA.

To raise antibodies against the C terminus of POB15 (amino acids 541-820), a portion of the *pob15* gene (nucleotides 1621-2460) was first PCR-amplified and subcloned in a pGEMT vector. The relevant fragment was then moved into a modified pGEX-6-P vector using the SpeI restriction site. The clone was subsequently sequenced verified.

A codon-optimized version of a portion of the *poc-16*(1-885) gene was synthesized by GeneArt (Life Technologies) using the *Escherichia coli* codon usage. The *poc-16*(1-885) gene was subsequently cloned in a modified pGEX-6-P vector using the SpeI restriction site. A positive clone in the good orientation was selected, sequence-verified and used to express the corresponding fusion protein.

## Protein expression and antibody production

The *E. coli* strain BL21(DE3) (Thermo Fisher Scientific) was used for protein expression. In general, bacteria were grown to an OD600 of 0.5 in LB medium at 37°C containing ampicillin. The temperature was switched to 20°C and the culture induced by the addition of isopropyl 1-thio-β-galactopyranoside (IPTG) to a final concentration of 0.5-1mM. Protein expression was performed at 20°C for 16 hr.

The fusion protein GST-POB15(541-820) was purified from inclusion bodies using the rapid GST inclusion body solubilization and renaturation kit (Cell Biolabs) at 4°C, according to the manufacturer's information. Recombinant purified GST-POB15 fusion protein (amino acids 541-820) was used to immunize a rabbit (Eurogentec). Antibodies were subsequently column-purified against the corresponding fusion protein. Briefly, 1 mg of purified GST-POB15(541-820) was bound to 350 mL of affigel-15 (Bio-Rad) for 4 hr at 4°C on a rotating wheel. 5 mL of serum was applied to the GST-POB15-bound affigel-15 column for 4 hr at 4°C. After extensive washing with PBS, antibodies were eluted with 350 mL 0.2M glycine pH 2.5, 0.5M NaCl and then neutralized with 1M Tris-HCl pH 8.0.

The fusion protein GST-POC16(1-295) was purified using glutathione agarose beads (Invitrogen). Briefly, the bacterial cell pellet was first resuspended in lysis buffer (50mM Tris pH 7.5, 300mM NaCl, 1mM DTT, proteases inhibitor cocktail, 5mM EDTA) and then incubated with 0.8 mL lysozyme at 10 mg/ml and DNase (supplemented with MgSO4 10mM) for 10 min on ice. After sonication, 0.5% Triton was added to the lysate prior to centrifugation at 12 000 g for 30 min. The resulting soluble lysate was incubated with glutathione Sepharose beads for 1 hr at 4°C on a rotating wheel. Beads were first washed with lysis buffer supplemented to 1M NaCl and 1% Triton and subsequently washed with lysis buffer. Elution of GST-POC16 was done in cleavage buffer (20mM Tris pH 7.5, 150mM NaCl, 0.5mM EDTA, 1mM DTT) overnight using 20 μL Prescission protease. The protein was dialysed overnight against PBS/5% glycerol. The purified protein POC16(1-295) was used to immunize a rabbit (Eurogentec). Antibodies against POC16 were column-purified using affigel 10 as described above and dialysed against PBS/10% glycerol.

## *Chlamydomonas* immunofluorescence and super-resolution

Isolated *Chlamydomonas* centrioles and procentrioles were centrifuged at 10 000 g (JS13.1 rotor, Beckman Coulter) onto a 12 mm coverslip (Roth, reference YX03.1) in a 15 mL Corex tube with an adaptor. Coverslips were then fixed for 7 min in –20°C methanol, washed in PBS, incubated 60 min at room temperature with primary antibodies in 1% bovine serum albumin and 0.05% Triton X-100, washed 15 min in PBS, and incubated 45 min at room temperature with secondary antibodies. Primary antibodies were 1:300 rabbit CrSAS-6 [19], 1:400 rabbit POB15 (this study), 1:400 rabbit POC16 (this study), 1:1000 rabbit PolyE (Adipogen, IN105), 1:200 mouse α-tubulin (Abcam, DM1A), 1:1000 mouse acetylated tubulin (Invitrogen) and 1:1000 mouse glutamylated tubulin (GT335, Adipogen). Secondary antibodies were 1:1000 goat anti-rabbit coupled to Alexa 568 and 1:1000 goat anti-mouse coupled to Alexa 488. Imaging was done on a 3D N-SIM/N-STORM Nikon microscope as described [19].

After SIM acquisition, 30 centrioles stained for α-tubulin and 30 centrioles stained for acetylated tubulin were used to measure the distance between the peaks of intensities.

2D Single Particle analysis of the SIM images was performed by automatically identifying centrioles using the algorithm described in [50]. The centrioles identified in this manner were subjected to 2D classification using CL2D [51]. Masks isolating each centriole from the centriolar-pair in the 2D classes were then defined, and subsequently applied to the images supporting each one of the classes. About 1000 centrioles have been extracted from 4 different experiments.

For specific proteins localization, 15 centrioles have been used for CrSAS-6, 18 centrioles for Bld10p, 31 centrioles for MonoE, 28 centrioles for POB15 and 22 centrioles for POC16.

To quantify the presence of different proteins/marker during centriole elongation, 54 procentrioles were analyzed for CrSAS-6/acetylated tubulin, 82 procentrioles for CrSAS-6 /MonoE, 54 procentrioles for acetylated tubulin /POB15 and 10 procentrioles for POB15 /MonoE.

## Immuno-EM

Isolated *Chlamydomonas* centrioles were spun on coverslips at 10 000 g using a JS13.1 rotor (Beckman) for 10 min and then fixed in 2% paraformaldehyde, 0.1% Glutaraldehyde in 0.1M phosphate buffer (PB), pH7.4. Coverlips were washed in PB three times for 5 min. Next, coverslips were blocked in PBS (0.01M, pH 7.4), 0.2% BSA and 5% NGS, 0.05% Triton X-100 for 60 min, and then washed in PBS (0.01M, pH 7.4), 0.2% BSA 0.02% Triton X-100 twice for 10 min and further incubated in primary antibodies (rabbit POB15 1:100) with PBS (0.01M, pH 7.4), 0.2% BSA, 0.02% Triton X-100, at 4°C overnight to ensure that the solution covered the coverslips. Next, coverslips were washed in PBS, 0.2% BSA three times for 5 min and subsequently incubated with 1:50 goat anti-rabbit secondary antibodies (Nanogold-IgG, Nanoprobes) in PBS, 0.2% BSA for 3-4h. Coverslips were washed in PBS, 0.2% BSA three times for 10 min, then twice for 10 min in PB, before post-fixation with 2.5% glutaraldehyde (0.1M, pH7.4) during 30 min. Afterward, the coverslips were washed in PBS once, then in distilled water four times for 10 min. Next, silver enhancement (HQ Silver, Nanoprobes) was performed at room temperature in the dark for 1 hr with 2 drops of developer to the final mix, checking staining under the light microscope. After washing in distilled water twice for 10 min and twice in PBS for 5 min, osmification was performed in 0.50% osmium tetroxide in PBS for 15 min. Finally, coverslips were dehydrated in a graded alcohol/distilled water series, 3 min each (twice in 50% ethanol, once in 70% ethanol, once in 90% ethanol, once in 95% ethanol and twice in 100% ethanol), and embedded in Durcupan using the same graded durcupan/ethanol series. Sections were imaged with a F20 microscope equipped with a 4kx4k FEI Eagle camera. Quantifications were done using 6 centrioles with a total of 36 gold beads.

### Cloning

Full-length WDR90RR-GFP was cloned in the Gateway compatible vector pEBTet-GW-EGFP [52]. The WDR90 DNA sequence was engineered to be RNAi-resistant (GeneCust, Europe) as such: position (534-554bp) 5′ACg AGc Gat CTc TGt TTc GAa 3′ and position (4971-4991bp) 5′ Tat AAa GAa GTc ATt ATa TAt 3′. Note also that for cloning purposes, the following restriction sites were mutated: AgeI (position 468bp) 5′AAt 3′ and NotI (position 3408bp) 5′ TGt GGC CGC CTG 3′. WDR90RR was first subcloned in pENTR using the restriction sites AgeI and XbaI. Second, a Gateway reaction was performed to generate the final expression plasmid pEBTet-WDR90RR, which was sequenced verified prior to transfection in human cells.

### siRNA of human cells and ciliogenesis

To generate the inducible episomal iRPE-1 p53-:WDR90RR-GFP cell line, RPE-1 p53- cells were transfected using Lipofectamine 3000 (Life Technology). Transfected cells were first selected for 10 days with 5 μg/ml puromycin, starting one day after transfection, and then with 20 μg/ml puromycin. Selected cells were then amplified and frozen.

Early passage cells were used for the experiments, inducing expression with 1 μg/ml doxycycline for 48 hr while depleting endogenous WDR90 using 50nM Silencer select pre-designed siRNA s47097 5′CCAGUGACCUGUGCUUUGAtt3′ (Thermo Fisher Scientific) that targets the beginning of the gene (Lipofectamine RNAiMAX, Thermo Fisher Scientific). Negative control siRNA (Thermo Fisher Scientific) was also used in parallel. Cells were then starved for 48 hr in low serum to induce ciliogenesis for 48 hr prior to fixation. Roughly 300 000 RPE-1 p53- cells control or expressing WDR90RR-GFP were plated on a 6-well plate.

The ciliogenesis assay presented in Figure 7H is from 3 independent experiments. 250 cells were counted per condition. The rescue experiment shown in Figure 7L is from 3 independent experiments. 50 cells counted per condition.

### Immunofluorescence microscopy of human cells

RPE-1 p53- cells grown on a 15 mm glass coverslips (Menzel Glaser) were fixed for 7 min in −20°C methanol, then washed once in PBS. Cells were incubated in 1% bovine serum albumin in PBST (PBS + 0.05% Tween-20) with primary antibodies against WDR90 (rabbit, 1:500, Novus, NBP2-31888), Centrin (mouse, 1:1000, 20H5), CP110 (rabbit, Lubios, 12780-1-AP, 1:500), Cep290 (rabbit, Lubios, A301-659A, 1:1000), TCTN1 (rabbit, Lubios, 15004-1-AP, 1:20) or Cep164 (rabbit, Lubios, 22227-1-AP, 1:200) and glutamylated tubulin (GT335, mouse 1:500, Adipogen) for 1 hr at room temperature. Coverslips were washed in PBS for 30 min prior to incubation with secondary antibodies (1:1000, goat anti-rabbit coupled to Alexa 568 and goat anti-mouse coupled to Alexa 568; both Life Technologies) for 1 hr at room temperature, washed again for 30 min in PBS and mounted in DAPCO mounting medium containing DAPI (Abcam). For quantification of primary cilia, only WDR90-overexpressing cells were considered for the analysis. Imaging was done on a Zeiss LSM700 confocal microscope with a PlanApo 63x oil immersion objective (NA 1.4) and optical sections were acquired every 0.33 μm, then projected together using ImageJ.

To quantify the distances between different centriolar markers, 39 centrioles were analyzed to measure WDR90 signal to Centrin, 22 centrioles for MonoE signal to centrin and 41 centrioles for CP110 signal to MonoE.

### CIB1 cassette mapping in *Chlamydomonas* mutants

Genomic DNA of isolated single clones for each mutant as well as the wild-type strain was performed using Chelex. Briefly, a solution of 5% Chelex resin was prepared in ddH2O (Chelex 100-grade resin, BIORAD). Each single colony from a plate was first resuspended in 20 μL ddH2O, followed by the addition of 20 μL 100% EtOH and 200 μL Chelex 5%. The mixture was vortexed and placed at 100°C for 8 min, then at 4°C for one minute. The samples were spun down at 16 000 g for five minutes in a tabletop centrifuge. Supernatants were collected and contained the extracted genomic DNA. 1 μL of the supernatant was used to perform subsequent PCR reactions. Sets of primers flanking the region of the putative CIB1 insertion site were chosen according to the Chlamylibrary website (https://www.chlamylibrary.org/). To map the cassette-genome junctions and the orientation of the cassette, we used the following primers in the CIB1 cassette: Cassette (1) and Cassette (2).

### Swimming assay

*Chlamydomonas* wild-type and mutant strains were grown in TAP medium 1X under light with agitation (180rpm) for 2-3 days prior to imaging. The swimming phenotype was recorded on an AxioplanZ1 microscope (Zeiss) with a 20X objective using a DIC filter (20ms time interval), and an Orca-Flash 4.0 LT camera (Hamamatsu).

### Flagella length measurements

Confocal images of the different wild-type and mutant strains were used to measure the length of flagella using ImageJ. Note that only straight flagella were measured. 37 flagella were measured for the wild-type, 28 flagella for m36, 17 flagella for m263, 25 flagella for m32, 39 flagella for m555 and 25 flagella for m504.

## QUANTIFICATION AND STATISTICAL ANALYSIS

Images were analyzed using ImageJ [48]. All statistical analyses were done using Excel and are provided in the figure legends and results. All data are expressed as the mean (average) +/− the standard deviation (SD). The value of n and what n represents (e.g.,

number of centrioles, number of replicates) is stated in figure legends and/or results. Two-tailed Student's t tests were performed for normally distributed data and are indicated in figure legends and/or results.

## DATA AND SOFTWARE AVAILABILITY

The accession number for the mass spectrometry proteomics data reported in this paper is ProteomeXchange Consortium PRIDE: PXD005818.

## ADDITIONAL RESOURCES

A website dedicated to the Mass Spectrometry analysis can be found here: http://pobdb.vital-it.ch/.